



# Reynolds analogy violation for a compressible turbulent boundary layer with pressure gradient in a small-size supersonic slot channel

N.A. Kiselev<sup>a,\*</sup>, N.S. Malastowski<sup>a,b</sup>, A.G. Zditovets<sup>a</sup>, Yu.A. Vinogradov<sup>a</sup>

<sup>a</sup> Lomonosov Moscow State University, Institute of Mechanics, 119192, Moscow, Michurinskiy Pros. 1, Russia

<sup>b</sup> Bauman Moscow State Technical University, 105005, Moscow, 2-Baumanskaya UL5, Russia



## ARTICLE INFO

### Keywords:

Adverse pressure gradient  
Non-equilibrium turbulent boundary layer  
Reynolds analogy  
Heat transfer coefficient  
Skin friction coefficient  
Adiabatic wall temperature

## ABSTRACT

Skin friction and heat transfer in compressible gas flow in a small supersonic slot channel were investigated. Experimental results describe the influence of weak and moderate non-equilibrium adverse pressure gradient (APG) on the skin friction  $c_f$  and heat transfer St coefficients, the Reynolds analogy factor  $s=2St/c_f$ , and the temperature recovery factor  $r$ . The pressure gradient value was controlled by the divergence angle of the supersonic section of the channel, resulting in variations in the pressure gradient parameter  $\beta_K$  in the  $-0.05 \dots 0.4$  range. The displacement thickness Reynolds number at the beginning of the APG region was  $Re^*=1300 \dots 2100$ , depending on the stagnation pressure in the plenum chamber. The experimental values of the skin friction coefficient were obtained using the Shapiro-Hawthorne method, while the heat transfer coefficient and adiabatic wall temperature were determined based on transient temperature fields recorded by an IR camera. For flows realized in the experiment, the solution of a system of steady-state two-dimensional boundary layer equations is considered. The values of the Reynolds analogy factor were compared with the values for an equilibrium boundary layer for the same pressure gradient parameter  $\beta_K$  and the Reynolds number  $Re^*$ . According to the results obtained, the state of the investigated boundary layer is significantly influenced by the history of its development. An upstream strong favorable pressure gradient in the supersonic nozzle required for producing supersonic flow in the channel leads to a reduction in the Reynolds analogy factor at the entry to the investigated region. In the investigated region downstream of the supersonic nozzle the skin friction and heat transfer coefficients and the Reynolds analogy factor were recovered up to the values of the equilibrium zero pressure gradient boundary layer. However, the  $s$  values were considerably lower than the equilibrium values for the same  $\beta_K$ . The maximum obtained value of the Reynolds analogy factor was independent of  $\beta_K$  in the experiments range and amounted to  $s \approx 1.0$ . Moreover, the difference from the equilibrium values starts to increase with an increase in  $\beta_K$ . The temperature recovery factor in the APG region corresponds to a fully turbulent flow.

## 1. Introduction

The description of heat transfer and skin friction laws in high-velocity gas flows has remained topical for a century [1]. The need to control boundary layer flows (for example, turbulence suppression for reducing the skin friction of the aircraft wings or heat transfer enhancement) and the estimation of the skin friction and heat transfer coefficients under external forces, including that of pressure gradients, so far keep up an interest in these investigations. Depending on the sign of the pressure gradient flows with an adverse (positive) pressure gradient (APG) and a favorable (negative) pressure gradient (FPG) are conventionally distinguished. Turbulent boundary layers (TBL) with an

APG can be encountered in both internal (diffusers) and external flows (wings of flight vehicles, gas turbine blades, wind turbine, etc.). These boundary layers are of fundamental interest, since, as distinct from zero pressure gradient (ZPG), they involve an additional force, apart from the skin friction. This force controls the process of the boundary layer formation [2,3] and enters the integral momentum equation in the form [4]:

$$\frac{d}{dx} (\rho_e U_e^2 \theta) = \underbrace{\tau_w}_{\text{shear stress}} + \underbrace{\delta^* \frac{dp}{dx}}_{\text{pressure gradient force per unit area}}, \quad (1)$$

where  $\rho_e$  is the density in the flow core,  $\text{kg/m}^3$ ,  $U_e$  is the velocity in the

\* Corresponding author.

E-mail address: [kiselev.nick.a@gmail.com](mailto:kiselev.nick.a@gmail.com) (N.A. Kiselev).

<b>Nomenclature</b>		<b>Criteria</b>
<i>A</i> and <i>B</i>	constants in velocity defect law, equation (2)	M Mach number
$A_\theta$ and $B_\theta$	constants in temperature defect law, equation (2)	$M_{av}$ mass flow averaged Mach number
$A_{ch}$ , $B_{ch}$ and $H_{ch}$	channel area, $\text{m}^2$ , width, m and height, m	$M_\pi$ Mach number calculated from the pressure gas-dynamic function
$c_f$ ( $c_f/2$ )	skin friction coefficients	$\text{Pe}_t$ turbulent Peclet number
$c_{f0}$ and $S_{t0}$	skin friction and heat transfer coefficients in an incompressible ZPG TBL with the same Reynolds number	$\text{Pr}$ Prandtl number
$c_p$	specific heat capacity at constant pressure, $\text{J}/(\text{kg}\text{K})$	$\text{Pr}_t$ turbulent Prandtl number
$dp/dx$	pressure gradient, $\text{Pa}/\text{m}$	$\text{Re}^*$ displacement thickness Reynolds number
$D_h$	hydraulic diameter, m	$\text{Re}_1$ unit Reynolds number, $1/\text{m}$
$E$ , $F$ , $E_v$ , $F_v$	flux vectors in equation (5)	$\text{Re}_0$ momentum thickness Reynolds number
$G$	mass flow rate, $\text{kg}/\text{s}$	$St$ Stanton number
$h$	specific enthalpy, $\text{J}/\text{kg}$	
$H$	boundary layer shape factor	
$k = 1.4$	specific heat ratio	
$p$	static pressure, Pa	
$p_0$	stagnation pressure, Pa	
$q$	isentropic flow function for flow rate	
$q_w$	heat flux, $\text{W}/\text{m}^2$	
$r$	temperature recovery factor	
$R$	specific gas constant, $\text{J}/(\text{kg}\cdot\text{K})$	
$s$	Reynolds analogy factor	
$T_0$	stagnation temperature, K	
$T_e$	temperature in the flow core, K	
$T_{aw}$	adiabatic wall temperature, K	
$T_w$	wall temperature, K	
$u$ , $v$	local values of the x- and y-velocity component, $\text{m}/\text{s}$ in the boundary layer	
$U_e$	velocity in the flow core, $\text{m}/\text{s}$	
$U_{95}$	uncertainties of measurements	
$x, y, z$	longitudinal, normal to the wall and transverse coordinates, m	
$y^+$	dimensionless distance from the wall	
<b>Subscript and superscript</b>		
$eq$	equilibrium value	
$\sum$	sum of viscous and eddy components	
$lam$	viscous component	
$turb$	eddy component	
$w$	value at the wall	
$\beta = 0$	ZPG TBL value	
$throat$	value at the throat	
$av$	mass flow averaged value	
<b>Greek symbol</b>		
$\kappa$	von Karman constant for the velocity law	
$\alpha$	heat transfer coefficient, $\text{W}/(\text{m}^2\text{K})$	
$\beta$	pressure gradient parameter	
$\beta_K$	parameter of the pressure gradient in compressible flow	
$\delta$	boundary layer thickness, m	
$\delta^*$	displacement thickness, m	
$\delta_K^*$	kinematic displacement thickness, m	
$\theta$	momentum thickness, m	
$\kappa_0 = 0.41/\text{Pr}_t$	von Karman constant for the temperature law	
$\lambda$	thermal conductivity, $\text{W}/(\text{m}\cdot\text{K})$	
$\mu$	dynamic viscosity, $\text{Pa}\cdot\text{s}$	
$\pi$	isentropic flow function for pressure	
$\rho$	local values of the density, $\text{kg}/\text{m}^3$ in the boundary layer	
$\rho_e$	density in the flow core, $\text{kg}/\text{m}^3$	
$\tau$	shear stress, Pa	
$\rho \bullet U$	mass flux, $\text{kg}/(\text{m}^2\text{s})$	
$\Psi_M$	compressibility correction factor	
<b>Designations</b>		
APG	adverse pressure gradient	
CFD	computational fluid dynamic	
DNS	direct numerical simulation	
FPG	favorable pressure gradient	
IR	infrared	
$k-\omega$ (SST)	shear-stress-transport turbulent model	
RANS	Reynolds-averaged Navier-Stokes	
TBL	turbulent boundary layer	
ZPG	zero pressure gradient	

flow core,  $\text{m}/\text{s}$ ,  $\tau_w$  is the shear stress at the wall, Pa, and  $dp/dx$  is the static pressure gradient,  $\text{Pa}/\text{m}$  along the longitudinal coordinate  $x$ , m. The displacement thickness  $\delta^*$  and the momentum thickness  $\theta$  are determined by integration of the boundary layer concerning the height:

$$\delta^* = \int_0^\delta \left(1 - \frac{\rho u}{\rho_e U_e}\right) dy \quad \text{and} \quad \theta = \int_0^\delta \left(1 - \frac{u}{U_e}\right) \frac{\rho u}{\rho_e U_e} dy$$

where  $\delta$  is the boundary layer thickness (the distance from the wall along the transverse coordinate  $y$ , m at which the velocity  $u = 0.995 \cdot U_e$ ), and  $\rho$  and  $u$  are the local values of the density,  $\text{kg}/\text{m}^3$ , and velocity,  $\text{m}/\text{s}$  in the boundary layer.

The pressure gradient influences the formation of both dynamic and thermal boundary layers, whose similarity is an important aspect in describing turbulent gas flows. "The similarity degree" is usually expressed in the value of the Reynolds analogy factor:  $s = (2 St/c_f)$ . In ZPG TBL  $s$  is near-unity and is determined mainly by the physical properties of a gas:  $s \approx \text{Pr}^{-2/3}$  [5]; (for the air  $s \approx 1.16-1.18$  [6]).

The parameter  $s$  relates the momentum loss by friction (the term "pumping power" is commonly used to describe the characteristics of heat exchange equipment) with the convective heat flux and allows estimating the efficiency of the heat transfer surfaces [7]. Reynolds analogy violation toward heat transfer is relevant in relation to heat transfer enhancement. Under ordinary condition, heat transfer enhancement is connected to a significantly greater increase in skin friction. This implies that reducing the total heat transfer area is accompanied by an increase in the number of heat exchange surfaces (for instance, the number of tubes in a shell-and-tube heat exchanger). Meanwhile, external action on the boundary layer, characterized by a violation of the Reynolds analogy toward heat transfer, make it possible to reduce both the area of the heat transfer surface and their number [7].

The reduction of heat fluxes to a greater degree than a decrease in skin friction is topical for many heat-stressed technical applications, such as gas turbine blades or nozzles of rocket engines.

In the context of high-speed boundary layers, the cumulative effect of the longitudinal pressure gradient can be divided into: the direct

influence of the pressure gradient at the prescribed section, the influence of boundary layer history, and the compressibility effect, which is connected to changes in the Mach number along the streamline.

**The direct effect and the equilibrium flow conditions.** Clauser was one of the first to normalize the second term on the right side of equation (1) for APG flows by introducing the pressure gradient parameter  $\beta = (\delta^*/\tau_w) \cdot (dp/dx)$  [2,8]. The use of the parameter  $\beta$  became generally accepted in studying the APG flows. The fundamental difference between  $\beta$  and other equivalent parameters used to describe gradient flows [3] lies in the possibility of formulating the requirements for the equilibrium flow introduced by Clauser [2] while describing turbulent isothermal incompressible two-dimensional boundary layers on flat surfaces. The equilibrium TBL is defined as the flow in which all the properties attain self-similarity (in most cases of the boundary layer it is the longitudinal velocity component  $U_e$ ) and are independent of the longitudinal coordinate.

The equilibrium condition for a turbulent boundary layer assumes that a self-similar velocity profile exists and the flow history can be neglected. This assumption allows us to generalize results for a wide class of problems (see, for example, [9–13]). In this case, the pressure gradient parameter  $\beta$  turns out to be the only independent variable

(apart from the characteristic Reynolds number) [9,12,14].

For turbulent boundary layers, except for certain limiting cases (for example  $Re \rightarrow \infty$  case), the complete similarity is impossible owing to the independence of the inner and outer boundary layer scales [4]. However, for flows with high Reynolds numbers, the outer region occupies the entire height of the boundary layer, and near-equilibrium conditions can be considered [2].

Mellor and Gibson [9] presented a solution for an equilibrium APG TBL consisting only of an outer (log and wake) region. The velocity profiles and the skin friction coefficients were obtained in the entire pressure gradient range  $\beta = -0.5 \dots \infty$ . The value  $\beta = -0.5$  corresponds to the equilibrium boundary layer with maximum acceleration. The maximum value  $\beta = \infty$  corresponds to the pre-separation boundary layer with an APG. In such a flow the wall shear stress tends to zero  $\tau_w \approx 0$  [15] and leading to the skin friction coefficient  $c_f = \tau_w/(\rho_e U_e^2/2)$  approaching zero for the flow with non-zero velocity in core  $U_e$ .

The study [9] was continued in So's work [12], where the energy equation was solved, together with the momentum equation for incompressible turbulent equilibrium boundary layer. The final expression for the Reynolds analogy factor  $s$  was written in the form:

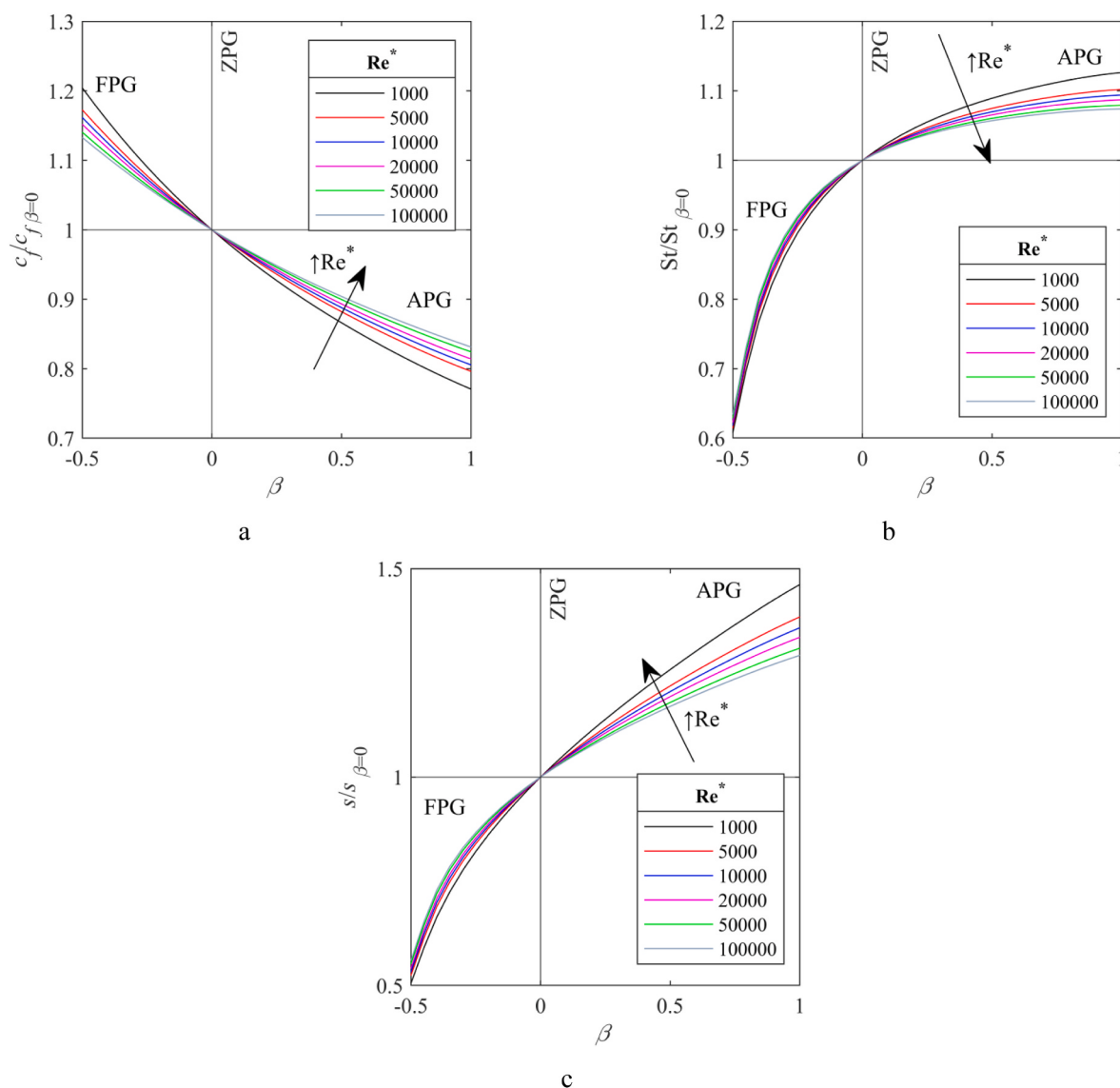


**Fig. 1.** Effect of the pressure gradient parameter  $\beta$  on the skin friction (a), heat transfer (b), and the Reynolds analogy factor at different Reynolds numbers  $Re^*$  (c) (calculated according to the mode [12]).

$$s = \frac{\kappa^{-1} \ln(\text{Re}^*) + B + A(\beta, \text{Re}^*)}{\kappa_{\theta}^{-1} \ln(\text{Re}^*) + B_{\theta} + A_{\theta}(\beta, \text{Re}^*)} \quad (2)$$

Here, the parameters of the log laws are  $\kappa = 0.41$ ,  $\kappa_{\theta} = 0.41/\text{Pr}_t$ ,  $B = 4.9$ , and  $B_{\theta} = 3.8$ . The velocity and temperature defects are characterized by the parameters  $A(\beta, \text{Re}^*)$  and  $A_{\theta}(\beta, \text{Re}^*, \text{Pr}_t)$ , respectively, which depend on the pressure gradient value, the Reynolds number, and the turbulent Prandtl number  $\text{Pr}_t$ .

The invariance of the equilibrium boundary layer parameters concerning to its formation makes it possible to conduct qualitatively (and sometimes quantitatively) analysis of the APG and FPG direct effects on the skin friction and heat transfer coefficients in relation to  $\beta$  and  $\text{Re}^*$  (Fig. 1). For an equilibrium boundary layer with constant Reynolds number  $\text{Re}^*$  (defined by displacement thickness  $\delta^*$ ), the Stanton number  $\text{St}$  increases, while the skin friction coefficient  $c_f$  decreases in flows with APG compared to ZPG case. This leads to an increase in the Reynolds analogy factor (up to  $s \rightarrow \infty$  at near separation condition, where the  $c_f$  value approaches zero while the  $\text{St}$  value remains finite, as heat transfer is determined only by thermal conduction). The opposite situation is typical for FPG conditions and leads to an increase in the skin friction coefficient and a decrease in the heat transfer coefficient. This results in a reduction of the Reynolds analogy factor  $s$  for accelerating flows.

Despite the fact that such flows are simple in mathematical description, their experimental implementation is extremely complex. These flows require consistency between the internal boundary-layer parameters ( $\delta^*/\tau_w$ ) with the pressure gradient  $d\rho/dx$ . Moreover, these flows are sensitive to the initial conditions and to the way in which the pressure gradient is imposed. The necessity of choosing the pressure gradient value in each section leads to a rather specific iterative procedure in the design of experimental channel since the displacement thickness and the wall shear stress are unknown beforehand. Aside from that, the development of an APG boundary layer leads to an increase in the Reynolds number. All the boundary layer parameters are influenced by  $\text{Re}^*$  and the equilibrium can be violated. Therefore, approximate equilibrium is often considered. Hence, the boundary layer parameters are measured at distances at which the flow history effect is neglected (about 50 boundary layer thicknesses [4]).

**The history effect.** Equilibrium flows can be considered only as limiting cases for real flows at given values of  $\beta$  and  $\text{Re}^*$ . Amount of studies indicated that with a sufficiently prolonged imposition of the APG, the boundary layer will develop into its equilibrium state [2, 16–18]. However, until it attains the equilibrium state it conserves the property associated with the flow history.

Flow history effects refer to various influences on the boundary layer that determine its condition in the given section. Its presence leads to a deviation from the equilibrium state and, as a consequence, to a deviation of the Reynolds analogy factor toward either heat transfer or skin friction. The boundary layer parameters differ from both initial and equilibrium values, even in non-equilibrium flows with  $\beta = \text{const}$ . For example, in Refs. [19,20] it was noted that at  $\beta \approx 2$  the Reynolds stresses in the outer region of a boundary layer are approximately half as large as in the equilibrium state [17], but they are higher than those in the ZPG case. As noted by Bradshaw [16], the flow history effects predominate in the outer part of the boundary layer.

Discussing initial flow characteristics related to boundary layer formation, initial ZPG [16], as well as FPG [19,21] region are considered. The initial ZPG conditions are realized to obtain the boundary layer thickness sufficient for carrying out the measurements and are achieved by the wind tunnel design. Particular attention should be paid to flows with the transition from FPG to APG. They can be encountered fairly frequently in supersonic nozzles, where the flows are characterized by low Reynolds numbers [22,23]. They are also present in the initial regions of pipes [24] and in flows around the blades of gas turbines [25–27]. In the region of preliminary acceleration of the flow, the pressure gradient parameter is significantly lower than the smallest value of  $\beta$  at which accelerated boundary layers can exist in equilibrium

[12]. An additional factor that requires to be taken into account is the gas flow compressibility since these flows are often transonic or supersonic.

**Compressibility effect.** Investigations of Reynolds analogy factor  $s$  in compressible flows are as interesting as similar studies in incompressible flows. In compressible flow, the  $\beta_K$  acts as a parameter of the pressure gradient instead of  $\beta$ :

$$\beta_K = \frac{\delta_K^*}{\tau_w} \frac{dp}{dx}.$$

It corresponds to  $\beta$  for the incompressible boundary layer. Here, the kinematic displacement thickness is used without taking into account the density variation across the boundary layer [28].

$$\delta_K^* = \int_0^\delta 1 - \frac{u}{U_e} dy.$$

This is since the use of the displacement thickness  $\delta^*$  leads to a several-fold increase in  $\beta$  with respect to  $\beta_K$  in compressible flows. The parameter  $\beta_K$  allows the use of the dependences obtained for incompressible flows in the entire range of experimental results.

Most of experimental setups are designed so that the greatest unit Reynolds number  $\text{Re}_1 = \rho \bullet U / \mu$ ,  $1/\text{m}$ , decreases with an increase in Mach number and the initial Mach number is limited to the  $M = 2 \dots 3$  range. Within the limits of the experimental accuracy, the treatment of compressibility [5,18,29–33] can be reduced to the Van-Driest transformation for velocity profiles [28,30,32] [29,31,33] [29,31,33] [28,30,32] and to the introduction of the compressibility correction factor. The decrease in the skin friction and heat transfer coefficients due to the variation in the gas density and temperature can be estimated, for example, from the expression [5].

$$\Psi_M = \frac{c_f}{c_{f0}} = \frac{\text{St}}{\text{St}_0} = \left( \frac{\arctg \left( M \sqrt{r^{\frac{k-1}{2}}} \right)}{M \sqrt{r^{\frac{k-1}{2}}}} \right)^2.$$

where  $c_{f0}$  and  $\text{St}_0$  - skin friction and heat transfer coefficients in an incompressible ZPG TBL with the same Reynolds number.

Compressibility, temperature recovery factor  $r$ , Mach number  $M$ , and the relationship between pressure losses due to skin friction and heat fluxes (Reynolds analogy factor) are also relevant for evaluating the efficiency of machine-free energy separation devices [34]. The efficiency of such devices increases with a decrease in the temperature recovery factor and an increase in the Reynolds analogy factor.

An important aspect of the experimental investigations of boundary layers is that in most studies the skin friction was not measured independently of the mean velocity profile. Instead, it was determined from the velocity profile slope in the log region of the boundary layer (Clauser method) [8]. However, in this case, the uniqueness of the results is missing: some authors assert that the APG affects the von Karman constant  $\kappa$  [19,20,35,36], whereas other authors affirm that this effect is absent [11,13,37]. It's worth noting that the answer is quite challenging since the measurement uncertainties can be greater than the effects under study, especially for high Reynolds number flows.

The solutions based on the computational fluid dynamic (CFD) approaches, including the direct numerical simulation (DNS), make it possible to obtain flows and flow parameters in conditions, where experimental investigations are not able to provide the desirable accuracy. Studies [18,33] devoted to the DNS of the boundary layer development under pressure gradient and the generalization of the results obtained for integral parameters. In Ref. [18] the heat transfer and skin friction coefficients were investigated in both compressible and incompressible boundary layers under near-adiabatic conditions. The DNS results for subsonic, near-incompressible flows are quite expected: the

skin friction coefficients are much more affected by the pressure gradient than the heat transfer coefficient. In a supersonic flow, the pressure gradient affects both  $c_f$  and St: even at  $\beta_K = 1.05$  the parameter  $s$  increases by 40% compared with the ZPG case, which is considerably greater than So's results [12] (Fig. 1). The authors noted a weak effect of the Mach and Reynolds numbers on the value of  $s$ . At the same time, additional differences are observable in the non-equilibrium flow region: whereas  $s$  follows accurately the equilibrium tendencies for subsonic cases, in supersonic flows the values of  $s$  are considerably lower in the APG and higher in the FPG compared to the equilibrium values.

We can note a significant amount of studies devoted to investigations of boundary layers under both adverse and favorable pressure gradients, including the non-equilibrium conditions. They demonstrated that the direct influence of the pressure gradient and compressibility effect can be accurately described mathematically. However, the history effect of the pressure gradient on dynamic and thermal boundary layers, especially in transitional conditions, holds significant scientific and practical interest for flows typical for nozzles and turbine blades. It means that the following aspects of the investigation require additional attention:

- development of compressible dynamic and thermal boundary layers. In these flows, history effects related to the strong FPG and the temperature and density variations across the boundary layer lead to a complicated physical behavior;
- experimental investigation of the skin friction and heat transfer. The influence of the APG on the dynamic boundary layer structure has been described fairly well. The experimental data on the APG effect on the skin friction and heat transfer coefficient and adiabatic wall temperature are insufficient owing to the complicity of their measurements;
- verification of the available numerical algorithms for calculating flows with non-equilibrium pressure gradients. At present, the mathematical methods of obtaining the data for engineering purposes predominate over experimental studies;
- systematization of the data on the sensitivity of integral parameters of the APG TBL for supersonic flows. Here, we can note the necessity of experimental and numerical studies of compressible non-equilibrium boundary layers in the absence of shock waves or wall curvatures.

Thus, the performance of experimental and numerical studies of the effect of weak and moderate non-equilibrium APG on the skin friction  $c_f$  and heat transfer coefficients St and, accordingly, the Reynolds analogy factor  $s$ , as well as the temperature recovery factor in compressible flows is an important scientific and practical challenge.

## 2. Methodology and objectives

The main aim of this study is an experimental investigation of heat

transfer and skin friction in a compressible boundary layer with an APG in a supersonic channel with strong preliminary flow acceleration where the development of an equilibrium TBL is impossible [12]. In such flows, it is necessary to consider the flow history effect (non-equilibrium FPG) on the boundary layers and the Reynolds analogy factor even at the entry to the investigated flow region with a pressure gradient.

It appears to be impossible to generalize the data obtained by the equilibrium boundary layers assumption in such flows. Therefore, a numerical solution of boundary layer equations for a steady two-dimensional flow has been used for analyzing the experimental data up to a shock. The results were compared with the equilibrium values from Mellor and Gibson [9] and the So solutions [12].

The experimental channel geometry is shown in Fig. 2 and consists of a supersonic nozzle, the investigated supersonic region with APG, and the diffuser. The channel height was chosen based on the features of the aerodynamic setup and the necessity to minimize the consumption of compressed air. An the same time, the following conditions were met: the channel width was sufficient to merge the boundary layers only at the exit from the supersonic region, and the ratio of the channel width to its height at the nozzle exit corresponded to recommended values [38]. The presence/absence of heat transfer on the opposite wall does not affect the thermal boundary layer on the wall under study. Moreover, a previous study [39] has shown that the heat transfer coefficient fields corresponded to the solution of three-dimensional RANS equations in the FLUENT software, and the growth of the boundary layer on the side (curved) walls of the channel didn't affect the flow until the shock formation region.

The nozzle geometry was taken from Ref. [40] with the isentropic Mach number  $M = 2.0$  [39]. The region under investigation was located downstream of the supersonic nozzle. Variation in the pressure gradient was achieved by varying the divergence angle of the supersonic region and was realized by replacing the channel. The supersonic nozzle geometry and, correspondingly, the upstream flow parameters of the investigated region were conserved.

The imposition of the pressure gradient was realized as follows. The variation of the Mach number (and all other flow parameters) along a streamline is possible when the sum of all effects on the flow (i.e. skin friction, area change, external heat change, or gas injection) is nonzero [41]. We considered only skin friction and area change:

$$\frac{dM^2}{M^2} = -\frac{2\left(1 + \frac{k-1}{2}M^2\right)}{1 - M^2} \frac{dA_{ch}}{A_{ch}} + \frac{k \cdot M^2 \left(1 + \frac{k-1}{2}M^2\right)}{1 - M^2} 4c_f \frac{dx}{D_H},$$

$$\frac{dp}{p} = \frac{kM^2}{1 - M^2} \frac{dA_{ch}}{A_{ch}} - \frac{k \cdot M^2 \left(1 + (k-1)M^2\right)}{2 \cdot (1 - M^2)} 4c_f \frac{dx}{D_H}$$

where  $A_{ch}$  is the channel cross-section area,  $m^2$ ,  $D_H$  is the hydraulic diameter,  $m$ , and  $p$  is the static pressure. In the constant area channel a

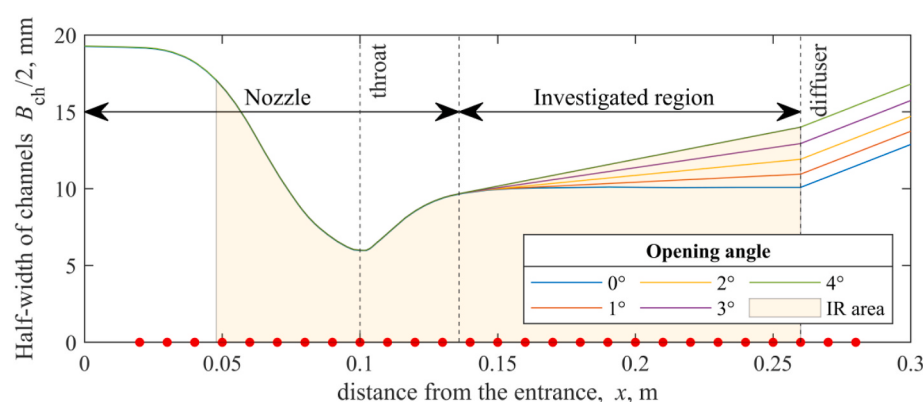


**Fig. 2.** Geometry of the investigated channels. Points present pressure taps. IR area presents the region covered with Zn-Se window.

decrease in the Mach number of supersonic flow and, accordingly, APG is observed due to the presence of skin friction. The flow in this channel corresponded to the highest APG value. An increase in divergence angle led to an APG reduction, down to a ZPG and a slight FPG. The supersonic flow in a convergent channel is accompanied by the shock waves. It makes the flow core essentially non-uniform.

The side walls of the supersonic region of the channel were made linear. The transition of the side walls from the nozzle to the supersonic channel was tangential. Consequently, the point of transition from the curved wall of the nozzle to the linear wall of the investigated region was shifted toward the throat with an increase in the divergence angle (from  $x = 0.1575$  m at  $0^\circ$  to  $x = 0.133$  m at  $4^\circ$ ). The divergence angle varied from  $0^\circ$  to  $4^\circ$  (Fig. 2). The near-ZPG condition was realized in the channel with a divergence angle of  $3^\circ$ .

### 3. Experiment and calculation

#### 3.1. Experimental setup

The experimental setup is shown in Fig. 3 [39,42]. The setup was supplied by compressed air from gasholders. The mass flow rate of air was regulated by a pressure-reduced regulator and measured by a Coriolis mass meter. Stagnation parameters (pressure and temperature) were measured after equalizing and calming the flow in the plenum. To minimize the effects of the boundary layer formed on the channel's side walls, a pre-insulated section extending 20 mm into the air-gate area (6) was installed.

The lower and upper walls of the channel are flat, the lower wall can be heated, while the upper one is replaceable. The heating is performed by hot propylene-glycol pumping along the backside of the lower wall. One of the removable upper walls was used to measure the static pressure distribution. The another one had an IR window (8), allowing temperature recording using the INFRATec 8800 IR camera (1). The window area covers the channel region from 0.05 to 0.26 m. The maximum difference between the adiabatic wall temperature  $T_{aw}$  and the lower wall surface temperature  $T_w$  did not exceed 50 K which enables the consideration of "near-adiabatic" boundary conditions. It means that the influence of the temperature factor on the parameters of the thermal and dynamic boundary layers is negligible, leaving only the impact of APG, along with the effect of flow compressibility.

The required mass flow rate is achieved by changing the stagnation pressure in the plenum chamber  $p_0$  at constant (atmospheric) pressure at the channel outlet. This led to variations in the flow density  $\rho$ , the unit Reynolds number  $Re_1 = \rho \cdot U / \mu$ , and the length of the supersonic flow region, up to the shock wave formation zone. In this study, we consider three flow regimes with values of  $p_0 \approx 2.25, 2.61$ , and  $3.02$  atm.

Heat transfer studies were carried out in all regimes, but data for  $p_0 \approx 3.0$  atm are presented as the most typical. The stagnation temperature varied from experiment to experiment in the range  $T_0 = 278.5 \dots 286.8$

K. Regulation of  $T_0$  was not carried out, since the effect of  $T_0$  changing in the obtained range on the experimental results is significantly lower than the measurement uncertainties.

#### 3.2. Experimental study

The experimental investigation was conducted in two stages:

**First stage:** The drained upper wall was installed to measure the static pressure along the channel length at different stagnation pressures in the plenum. The lower wall was not heated. The flow parameters were obtained using the measured values of static pressure, air flow rate, and pressure in the plenum. Mach number as a function of the streamwise coordinate  $x$  was calculated from the pressure gas-dynamic function:

$$\pi(M_\pi) = \frac{p}{p_0} = \left( 1 + \frac{k-1}{2} M_\pi^2 \right)^{\frac{1}{k-1}}, \quad (3)$$

where  $k = 1.4$ . The evaluated Mach number  $M_\pi$  (3) represents the maximum value within a section (specifically, the Mach number at the channel axis) under the condition that the stagnation pressure is conserved.

The well-known one-dimensional Shapiro-Hawthorne method was used to determine the skin friction coefficient [43]. The primary concept of this method is that the simultaneous change in all flow variables are expressed through a linear combination of independent action. Here, skin friction and area change are considered. By employing the conservation equations and the equation of state, the equation for the change in Mach number could be written as follows:

$$\frac{dM_{av}^2}{M_{av}^2} = - \frac{2 \left( 1 + \frac{k-1}{2} M_{av}^2 \right)}{1 - M_{av}^2} \frac{dB_{ch}}{B_{ch}} + \frac{k \cdot M_{av}^2 \left( 1 + \frac{k-1}{2} M_{av}^2 \right)}{1 - M_{av}^2} 4c_f \frac{dx}{H_{ch}}, \quad (4)$$

where  $B_{ch} = B_{ch}(x)$  is the channel width, m,  $H_{ch}$  is the channel height, m. Here, the mass flow averaged Mach number  $M_{av}$  is determined using the measured mass flow rate, stagnation parameters, and the distribution of static pressure along the length of the channel and its geometry defined by:

$$G = 0.0404 \cdot \frac{p_0}{\sqrt{T_0}} \cdot H_{ch} \cdot B_{ch} \cdot \frac{q(M_{av})}{\pi(M_{av})}, \text{ where}$$

$$q(M_{av}) = \frac{k+1}{2} M_{av}^2 \left/ \left( 1 + \frac{k+1}{2} M_{av}^2 \right)^{\frac{k+1}{2(k-1)}} \right.$$

Here  $G$  is mass flow rate, kg/sec,  $T_0$  is stagnation temperature, K. The skin friction coefficient  $c_f$  was calculated from (4) according to the experimental distribution of the Mach number  $M_{av}$ . This method enables the estimation of the skin friction coefficient  $c_f$  with acceptable accuracy and is applicable in experimental studies of high-speed flows [44]. To see an example of using this method, one could refer to section 6.2 of the study [41].

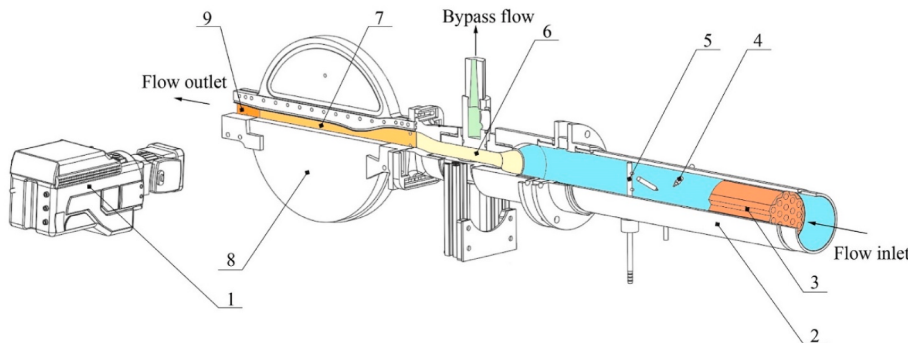


**Fig. 3.** Experimental setup: 1, IR camera; 2, plenum chamber; 3, honeycomb; 4, stagnation temperature probe; 5, stagnation pressure probes; 6, air-gate; 7, slot channel; 8, Zn-Se window, 9 – diffuser.

**Second stage:** the upper wall equipped with an IR window was mounted. The heat transfer coefficients ( $St$  and  $\alpha$ ) and temperature recovery factor  $r$  were investigated at the same stagnation pressures as in the first stage (Fig. 4). When the air gate (6) connected the plenum chamber directly with the atmosphere, the required air flow rate  $G$ , stagnation pressure  $p_0$ , and the constant temperature  $T_0$  were reached. The investigated wall of the channel was pre-heated using a hot coolant. Once the steady-state flow regime was reached, the incoming air was directed into the channel through the air gate (6). The cooling rate of the channel wall was measured using an IR camera (the sequence of the temperature fields of the surface under study was registered).

The heat transfer coefficients and adiabatic wall temperature were determined using the transient heat transfer method. For each point of the lower wall, a time-dependent heat flux corresponding to the experimentally measured cooling rate and the temperature of the back surface were calculated. The heat transfer coefficient (Fig. 4a) was determined as the ratio of the heat flux  $q_w$  to the temperature difference ( $T_{aw}-T_w$ ). The temperature  $T_{aw}$  corresponded to the linear extrapolation of the  $q_w(T_w)$  curve to the point  $q_w(T_{aw}) = 0$ . In more details, the method was described in Ref. [39]. The Stanton  $St$  number was calculated based on heat transfer coefficient  $\alpha$  and the measured mass flow rate  $G$ . The temperature recovery factor  $r$  (Fig. 4b) was evaluated using on stagnation temperature  $T_0$ , the local values of adiabatic wall temperature  $T_{aw}$ , and the distribution of Mach number  $M_\pi$  along the channel axis:

$$r = \frac{\frac{T_{aw}}{T_0} \left( 1 + \frac{k-1}{2} M_\pi^2 \right) - 1}{\left( 1 + \frac{k-1}{2} M_\pi^2 \right)}$$

It should be noted that the difference between the adiabatic wall temperature  $T_{aw}$  and the stagnation temperature  $T_0$  was insufficient and

the method of determining the recovery factor  $r$  presented above possessed considerable uncertainty in the flow region with a low Mach number ( $M < 1$ ). Therefore, this region is not shown in Fig. 4b.

### 3.3. Measuring uncertainty

The uncertainty of the key parameters obtained in this study was estimated for a 95% confidence level using the method presented in Ref. [45]. The main parameters of uncertainties analysis are presented in Table 1.

### 3.4. Numerical study

The simplest mathematical model taking into account the flow history was used to numerically evaluate the experimental results. The system of equations governing a steady two-dimensional boundary-layer flow in a narrow channel, which expresses the laws of conservation of mass, momentum, and stagnation enthalpy, can be written in the form [46]:

$$\begin{aligned} \frac{\partial \rho u B_{ch}(x)}{\partial x} + H_{ch} \frac{\partial \rho v}{\partial y} &= 0, \quad \frac{\partial \rho u \cdot u}{\partial x} + \frac{\partial \rho v \cdot u}{\partial y} = \\ - \frac{\partial}{\partial x} \left( \frac{\rho_e U_e^2}{2} \right) + \frac{\partial \tau^\Sigma}{\partial y}, \quad \frac{\partial p}{\partial y} &= 0, \quad \frac{\partial \rho u \cdot c_p T}{\partial x} + \frac{\partial \rho v \cdot c_p T}{\partial y} = \\ - u \frac{\partial}{\partial x} \left( \frac{\rho_e U_e^2}{2} \right) + \frac{\partial}{\partial y} (\tau^\Sigma u) + \frac{\partial}{\partial y} \left( \lambda^\Sigma \frac{\partial T}{\partial y} \right), \end{aligned} \quad (5)$$

where  $h = c_p T$ ,  $\tau^\Sigma = \mu^{lam} \frac{\partial u}{\partial y} + \mu^{turb} \frac{\partial u}{\partial y}$ ,  $\lambda^\Sigma = \lambda^{lam} + \frac{\mu^{turb} c_p}{Pr_e}$ .

This system (5) is closed by the equation of state for a perfect gas and is identical in form to the boundary layer equations but the boundary

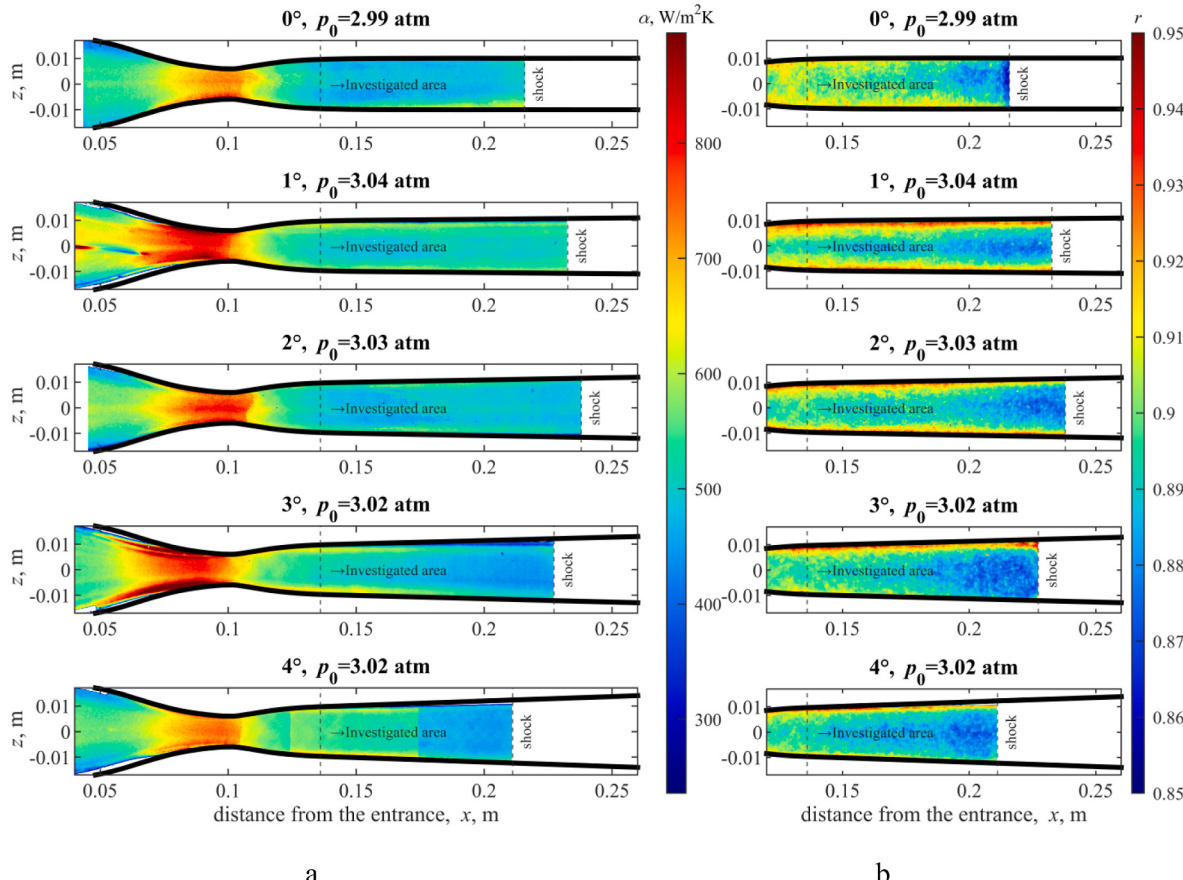


Fig. 4. Experimental fields of the heat transfer coefficient (a) and the temperature recovery factor (b) at  $p_0 \approx 3.0$  atm.

**Table 1**

Uncertainty values for measured quantities.

Variable	Value		$U_{95}$		Comments
	min	max	min	max	
$p_0$ , atm	2.20	3.06	$1.9 \cdot 10^{-2}$		Value is measured in plenum
$T_0$ , K	278.5	286.8	0.3		
$p$ , atm	0.36	2.97	$0.5 \cdot 10^{-2}$	$1.9 \cdot 10^{-2}$	
$G$ , g/s	24.1	36.6	0.12	0.18	
$M_\infty$	0.17	1.95	0.01	0.04	$U_{95}$ increases with a decrease $p_0$ and $M$
$M_{av}$	0.17	1.85	0.001	0.03	Calculated value
$\beta_K$	-1.12	0.4			Max $T_w$ is at the initial time of the experiment, min $T_w$ is at the end of the experiment
$T_w$ , K	266.7	330.4	0.6		
$T_{aw}$ , K	263.3	282	1		Max $T_{aw}$ is in subsonic, min $T_{aw}$ is in supersonic region
$r$	0.84	0.97	0.051	0.0024	$U_{95}$ increases significantly with a decrease in $M$ ( $U_{95} = 0.011$ at $M = 1$ , $U_{95} = 0.051$ at $M = 0.6$ )
$\alpha$ , W/ $m^2 \cdot K$	400	800	20	50	$U_{95}$ decreases with a decrease flow rate
$St$ , $10^{-3}$	0.95	2.3	0.065	0.19	Max of $St$ is in the subsonic region, min $St$ is in the throat
$c_f \cdot 10^{-3}$	1.9	3	0.018	0.4	$U_{95}$ decreases with a decrease in $M_{av}$

conditions on the external boundary of the computation domain (symmetry axis) must be obtained as a part of the solution. At the symmetry axis, the transverse velocity  $v$  and the transverse gradient of the longitudinal velocity  $du/dy$  must turn to zero. Since the channel walls are impermeable, the velocity in the flow core  $U_e$  was defined by area change (slot channel with  $B_{ch}=B_{ch}(x)$  and  $H_{ch} = \text{const}$ ) at a constant mass flow rate  $G$ . The stagnation pressure losses along the channel axis are determined by skin friction on the upper and the lower channel walls [41]. Thereafter the static pressure is calculated from the stagnation pressure using the correlation for isentropic flow at each section.

The formulation presented in this study does not take into account a shock formed in the flow, as well as boundary layer separation. Since this study is focused on the compressible boundary layer and the APG effect on the integral parameters, this problem was excluded from consideration. Moreover, we chose such approach because it will let us opportunity to get profile of nozzles with near-equilibrium condition using iterative procedure base on this simple model along marching coordinate in a future.

The turbulent component of the shear stress is determined by the  $k-\omega$  (SST) turbulence model [47]. The turbulent Prandtl number is defined using the correlation proposed by Weigand et al. [48].

$$\frac{1}{Pr_t} = \frac{1}{2Pr_{t\infty}} + 0.3Pe_t \sqrt{\frac{1}{Pr_{t\infty}} - (0.3Pe_t)^2} \left[ 1 - \exp\left(-\frac{1}{0.3Pe_t \sqrt{Pr_{t\infty}}}\right) \right],$$

where the Prandtl number in the flow core is taken to be  $Pr_{t\infty} = 0.85$ .

The equations were discretized using the finite-differences method and the marching approach in the streamwise coordinate [49]. This formulation of a numerical model reduces the computational time for the boundary layer calculations.

The computational domain consisted of half the channel with the pre-included region of 0.32 m in total length and 1.9 mm in height. A uniform grid had 801 grid points in length and 4001 grid points in height. The  $y^+$  at the first grid point from the wall was 0.3 in the APG region and 0.8 in the throat.

Two simulations were conducted to evaluate the heat transfer coefficient for each stagnation pressure. Each flow regimes were computed under adiabatic conditions ( $q_w = 0$ ) and with “near-adiabatic” fixed wall heat flux ( $q_w = \text{const}$ ). In the former case the parameters of the dynamic

boundary layer were determined, together with the adiabatic wall temperature  $T_{aw}$ , while in the latter case, it was the parameters of a thermal boundary layer and the heat transfer coefficient.

The calculated value of skin friction coefficient  $c_f$  was determined by

$$c_f = \frac{2 \cdot \tau_w}{\rho_e \cdot U_e^2},$$

where the shear stress was determined by the wall parameters  $\tau_w = \mu_w \cdot du/dy$ , and the density  $\rho_e$  and velocity  $U_e$  were taken in the flow core. The heat transfer coefficient  $St$  was determined by

$$St = \frac{q_w}{\rho_e \cdot U_e (T_w - T_{aw}) \cdot c_p},$$

where  $T_{aw}$  is taken for the regime of adiabatic flow, and parameters on the wall  $q_w$  and  $T_w$  are taken for the case with  $q_w = \text{const}$ . Since in the second case “near-adiabatic” conditions were considered, the flow core parameters  $\rho_e$  and  $U_e$  coincided with the values in an adiabatic flow. The calculated value of temperature recovery factor  $r$  was determined as  $r = (T_{aw} - T_e)/(T_0 - T_e)$ , where  $T_e$  and  $T_0$  are the static and stagnation temperatures in the flow core.

The computational model had been verified by comparing with experiments data and the results of modeling three-dimensional RANS equations in the FLUENT [39] (Fig. 5). The data obtained corresponded to the flow regime with  $T_0 = 278.3$  K and  $p_0 = 3.05 \cdot 10^5$  Pa in a channel with a divergence angle of  $3^\circ$ ; the wall temperature was  $T_w = 298.3$  K.

The results of the FLUENT calculations (the values in the symmetry plane of the channel) and the boundary layer equations coincided up to the section, in which a shock was observable, except for the non-uniformity of the 3D calculation result owing to the presence of characteristics in the supersonic flow region. The only difference was in the temperature recovery factor  $r$  distribution in the flow acceleration region. According to the FLUENT results,  $r$  decreased monotonically along the longitudinal coordinate. In the presented model considerable flow acceleration led to a decrease in the temperature recovery factor in the vicinity of the throat. Downstream  $r$  was recovered to ZPG turbulent value. The difference in the obtained values did not exceed the experimental uncertainties. Hence, both mathematical models can be treated as accurate.

We calculated flows in the full-height channel with different boundary conditions for the energy at the upper wall. The variation in heat transfer conditions on the opposite wall did not affect the boundary layer development on the investigated wall. The calculated boundary layer thickness did not exceed half of the channel height, except from the  $x > 0.25$  m region for the channels with the divergence angles of  $0-1^\circ$ .

## 4. Results and discussion

### 4.1. Parameters in the flow core

**Static pressure distribution.** The flow in the channel was controlled by the stagnation pressure  $p_0$ . The nozzle was choked at the pressure  $p_0 \approx 1.4$  atm. As  $p_0$  increased a shock moved toward the channel exit. This can be observed by comparing the relative static pressure distributions  $p/p_0$  for each investigated channel in Fig. 6a–c. As mentioned above, the initial section location of the investigated region depended on the divergence angle (Fig. 2). Hence, shock reached the investigated region at different  $p_0$  in channels. This pressure increased with a decrease in the divergence angle from 1.85 atm for a channel with the divergence angle of  $4^\circ$  to 2.19 atm for the channel of constant cross-section. The unit Reynolds number  $Re_1$  and mass flow rate  $G$  also increased. Fig. 6c shows the distribution of  $p/p_0$  at  $p_0 \approx 3$  atm. With a further increase in stagnation pressure, the position of the shock remains unchanged. As can be noted, supersonic flow could not be realized for channels with divergence angles  $0^\circ$  and  $4^\circ$  along the entire length (since it was greater than the critical length) of the investigated channel due to

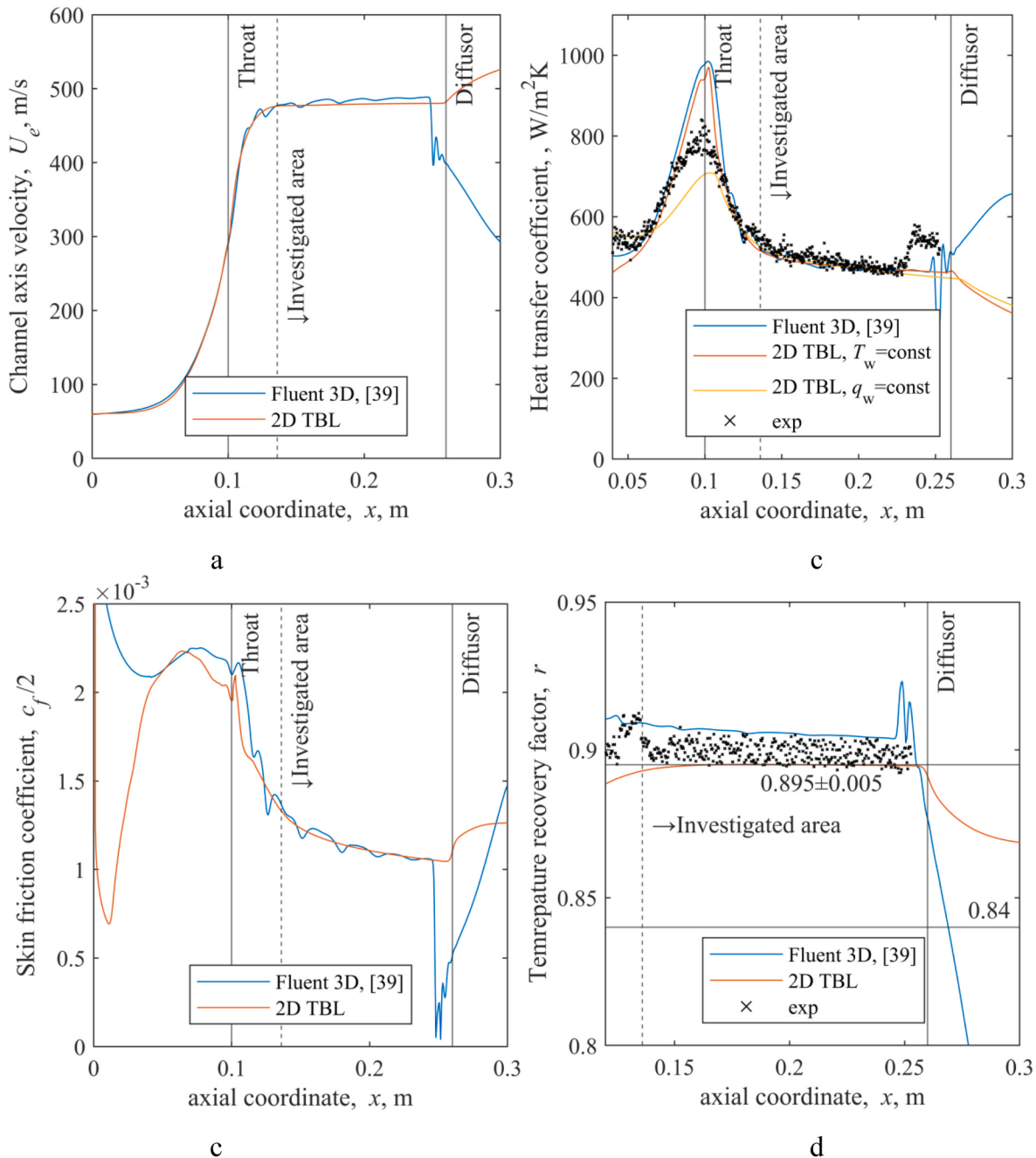


**Fig. 5.** Comparison of the FLUENT calculations [39] with the in-house 2D TBL code and the experiment.

physical limitations [41].

The area change started to compensate effect of skin friction, as the divergence angle increased. This shifted shock downstream at the same stagnation pressure  $p_0$ . This can be observed by comparing the distributions of  $p/p_0$  in Fig. 6a and b for channels with divergence angles 0–3°. However, an increase in the cross-section area led to a rise in the Mach number and the stagnation pressure losses in the shock. This reduced the supersonic flow region for the channel with the divergence angle of 4°, which can also be observable in Fig. 6a–c: the position of the shock for this channel is close to the constant area channel. Numerical and experimental values of the relative pressure  $p/p_0$  coincided throughout the entire investigated region, up to the shock.

The distributions of all dimensionless parameters (except the Reynolds number  $Re^*$ ) before the shock don't depend on the value of  $p_0$  (except for the influence of  $Re^*$ ). Therefore, it's possible to generalize

and present the results within a single regime  $p_0 \approx 3$  atm.

The **Mach number distribution** along the channel axis at the stagnation pressure  $p_0 \approx 3.0$  atm is presented in Fig. 7a and the corresponding calculated values of the longitudinal velocity  $U_e$  at the channel axis are shown in Fig. 7b.

The Mach number  $M_\pi$  at the nozzle exit (at the entry in the investigated section) was  $M_\pi = 1.86$  ( $U_e = 475$  m/s), which is lower than the isentropic Mach number  $M_\pi = 2.0$ . This is due to the presence of the boundary layer on the channel walls.

In the absence of area change (channel with zero divergence angle), the Mach number variation along the channel length is determined only by the skin friction coefficient. In this case, there is a decrease in the core flow velocity  $U_e$  to 407 m/s at the section  $x = 0.242$  m, where the boundary layers merge and then the flow core velocity starts to increase. However, as seen in Fig. 7a, the shock occurs earlier. The lowest

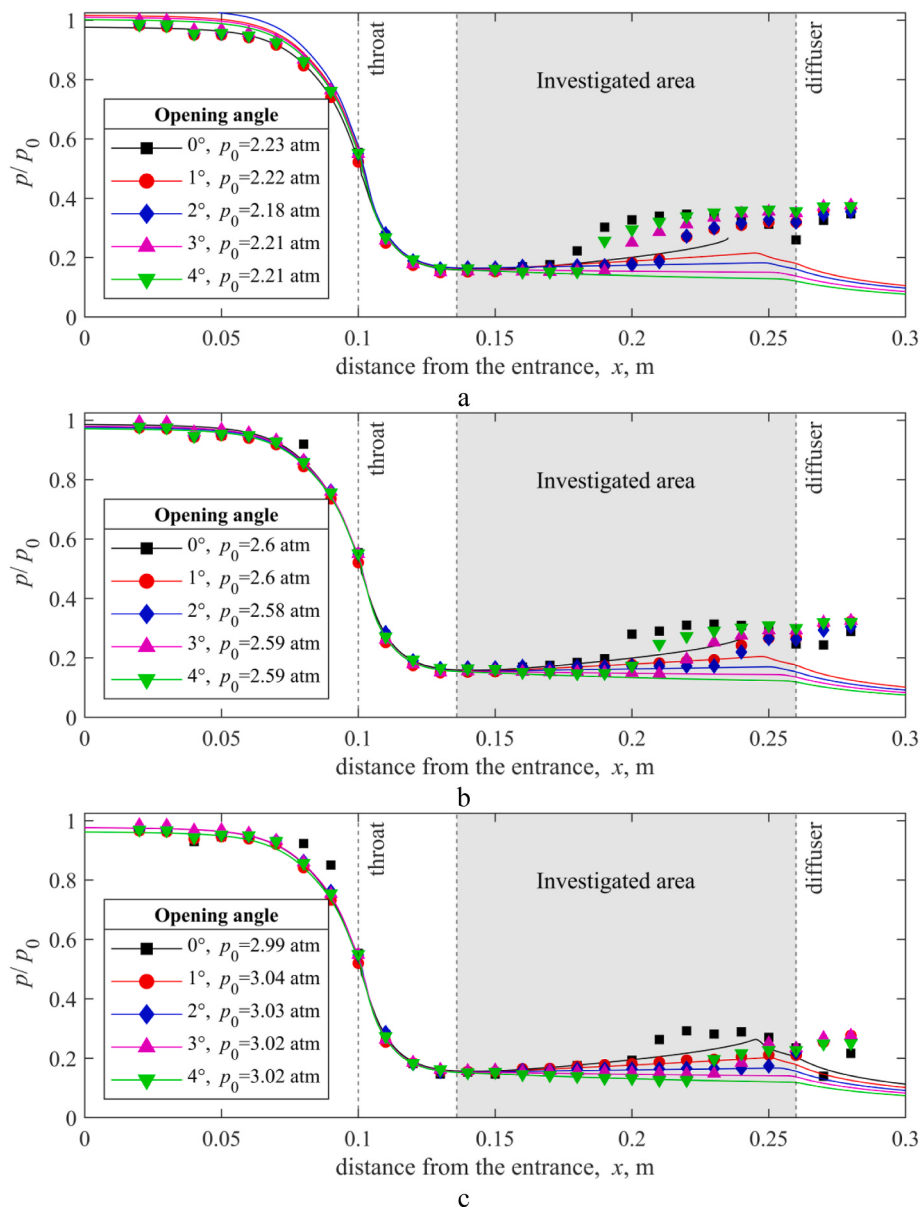


**Fig. 6.** Distribution of the relative static pressure  $p/p_0$  in the investigated channels at different stagnation pressures:  $p_0 \approx 2.2$  atm (a),  $p_0 \approx 2.6$  atm (b),  $p_0 \approx 3.0$  atm (c). Points present experimental data, lines present calculations.

experimentally determined Mach number for the channel with the largest APG reduced to  $M = 1.5$ .

With the increase in the divergence angle (to  $1\text{--}2^\circ$ ) the flow deceleration became less intense and the point of the merge of the boundary layers shifted toward the outlet. A flow with a constant flow core velocity is observed in the channel with the divergence angle of  $3^\circ$ . The highest Mach number in the channel with a slight acceleration (with the divergence angle of  $4^\circ$ ) was  $M = 1.95$  and the velocity was  $U_e = 500$  m/s.

**Pressure gradient parameter**  $\beta_K$  was almost independent of the stagnation pressure  $p_0$  in the plenum chamber but, required determination of the integral boundary-layer parameters. The displacement thickness  $\delta^*$  was not measured and the  $\beta_K$  was available only from an analysis of the numerical results. The distribution of the calculated value of  $\beta_K$  in the investigated channels (without accounting for shock) is presented in Fig. 8.

As noted above, despite the considerable length of the supersonic nozzle most of the flow acceleration (as noted in Ref. [12]) occurred at the values  $\beta_K < -0.5$ . This value is less than the minimum value, at

which an equilibrium boundary layer could be realized. Therefore, it can be expected that the boundary layer parameters will be far from the equilibrium values at the entry to the investigated region. This is characteristic of most supersonic channel flows, in which supersonic velocities are achieved due to area change.

In the investigated flow region weak flow acceleration can be observed for the channel with the divergence angle of  $4^\circ$  and  $\beta_K \approx -0.06$ , while in the channel with the divergence angle of  $3^\circ$   $\beta_K \approx 0$ . In the channel with zero divergence angle, the pressure gradient parameter is essentially non-uniform and increases, as the boundary layer grows. This is due to an increase in the displacement thickness and a decrease in the shear stress on the wall.

**Estimation of the mass flux, Reynolds number, and compressibility.** When the throat of a supersonic nozzle is choked, the mass flow rate through the nozzle is governed by the throat area ( $H_{ch} \cdot B_{ch}$ )<sub>throat</sub>, the stagnation parameters  $p_0$ ,  $T_0$ , and gas properties  $k$ ,  $R$ :

$$G = \frac{p_0 \cdot (H_{ch} \cdot B_{ch})_{throat}}{\sqrt{T_0}} \sqrt{\frac{k}{R}} \left( \frac{k+1}{2(k-1)} \right)^{\frac{k+1}{2(k-1)}},$$

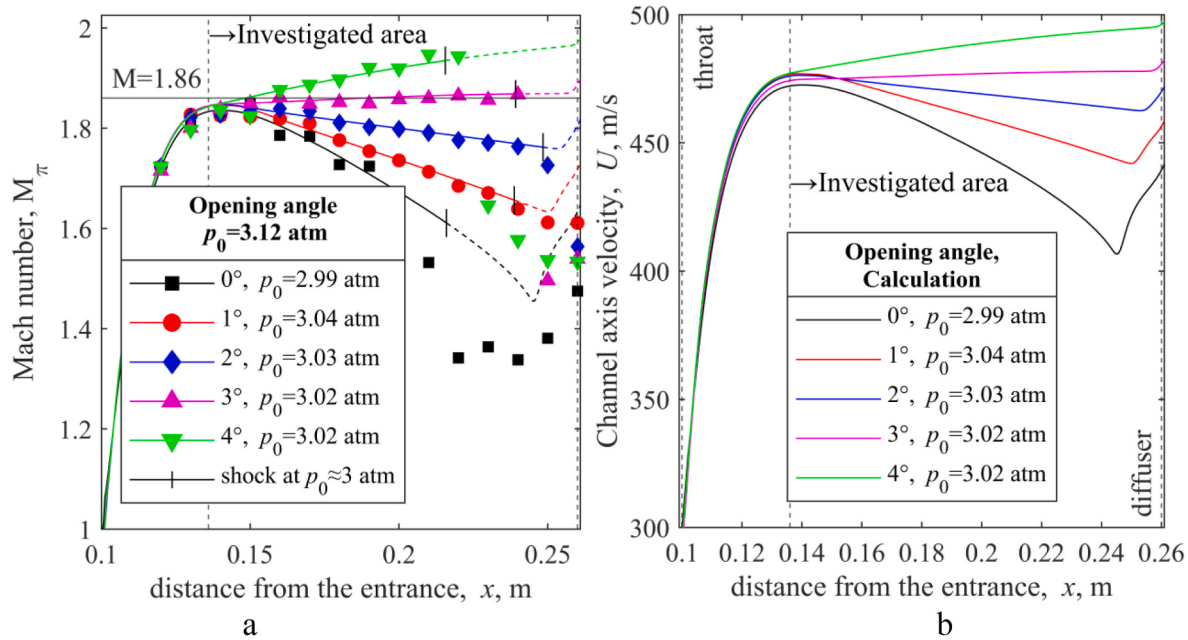


**Fig. 7.** Mach number (a) and velocity (b) distributions along the channel axis. Points present experimental data, lines present calculations.

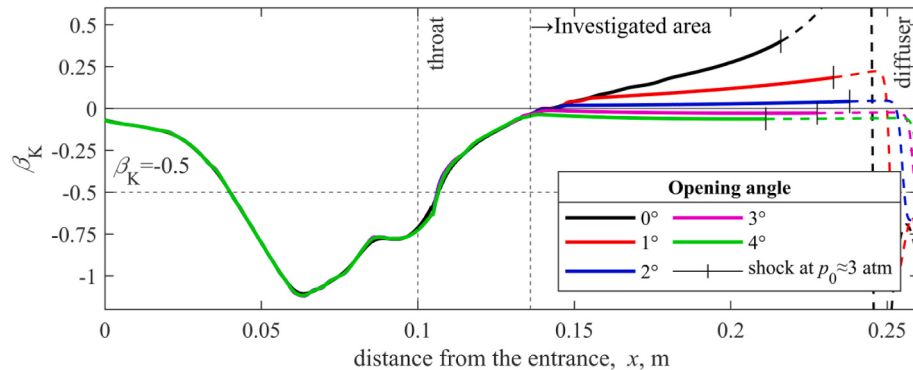


**Fig. 8.** Variation of the calculated pressure gradient parameter  $\beta_K$  along the channel length.

where  $R$  is the specific gas constant, J/kg•K. Therefore, mass flux  $(\rho \bullet U)_{av}$  increases with a decrease in the divergence angle of the supersonic region of the channel at a constant flow rate ( $G = (\rho \bullet U)_{av} \bullet H_{ch} \bullet B_{ch} = ((\rho \bullet U)_{av} \bullet H_{ch} \bullet B_{ch})_{throat} = \text{const}$ ). This leads to an increase in the Reynolds numbers and the heat transfer coefficient ( $\alpha = St \bullet \rho_e \bullet U_e \bullet c_p$ , W/m<sup>2</sup>K, where  $c_p$  is the specific gas heat capacity, J/kg•K) at a fixed Stanton number  $St$  (Fig. 4). It is worth noting that flow

core parameters are used in determining the heat transfer coefficient, and only mass-averaged parameters  $(\rho \bullet U)_{av}$  can be extracted from the condition of constant flow. These quantities are not directly proportional due to density changes across the boundary layer, but their change with the divergence angle is the same.

According to the calculation, with an increase in the pressure gradient, the displacement thickness Reynolds number  $Re^* = \rho_e \bullet U_e \bullet \delta^*/$

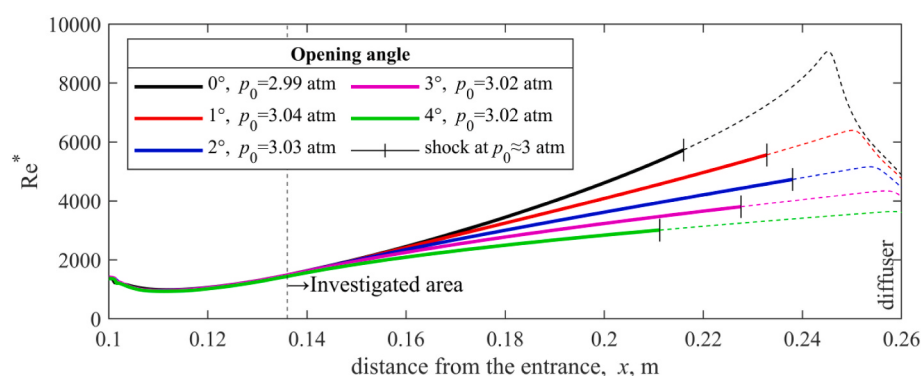


**Fig. 9.** Calculated Reynolds number  $Re^*$  distribution over channels length at  $p_0 \approx 3$  atm.

$\mu_w$  (the variation of the Reynolds number along the length of the channels at  $p_0 \approx 3$  atm is shown in Fig. 9) increased by a factor of up to 2.2 compared with the ZPG flow in the same section. Apart from the influence of the mass flux  $(\rho \cdot U)_{av}$ , this was due to the growth of the displacement thickness in the channel with the APG. The same behavior was characteristic for the momentum thickness Reynolds number  $Re_\theta$  (at a constant boundary layer shape factor  $H = \delta^*/\theta$ ). Such an increase in the Reynolds number  $Re_\theta$  (or  $Re^*$ ) led to a decrease in the skin friction and heat transfer coefficients up to 1.3 times.

We also note the Mach number variation along the length of a channel with a pressure gradient and its effect on the compressibility effect. A decrease in the Mach number in a channel with zero divergence angle resulted in an about 10% increase in  $\Psi_M$  and the skin friction and heat transfer coefficients.

#### 4.2. Parameters of dynamic and thermal boundary layers

As shown in the studies [9,12], heat and momentum transfer are sensitive to the pressure gradient in the limiting case of the equilibrium boundary layer: the skin friction coefficient decreases in the APG region, whereas the heat transfer coefficient increases (Fig. 1). Within the investigated range of  $\beta_K$  parameters, this effect does not exceed 10%. Nevertheless, it can be expected that non-equilibrium pressure gradient will lead to a reduction in the APG impact. Other factors, such as the increase in  $Re^*$  and the decrease in Mach number, compensate for each other in our investigated conditions and geometries (Fig. 2).

As will be shown below, the method of the experimental determination of the skin friction and heat transfer coefficient has significant uncertainty in comparison with the total effect of the pressure gradient.

**Skin friction coefficient.** Variations in the skin friction coefficient  $c_f$  (calculated and experimental data) along the channel length at  $p_0 \approx 3$  atm are presented in Fig. 10. In our case, the numerical values of the skin friction coefficients lie within the experimental data confidence level up to the shock waves, within the limits of the measurement uncertainty.

According to the calculation, the skin friction coefficient reduces as the boundary layer grows along the streamwise coordinate  $x$  and the pressure gradient increases due to the reduction of the divergence angle. However, in most cases, the  $c_f$  reduction in the APG is due to an increase in the Reynolds number  $Re^*$  relative to the Reynolds number for ZPG flow in the same longitudinal coordinate. A decrease in the Mach number (the compressibility effect) has the opposite effect and leads to an increase in  $\Psi$  and the skin friction and heat transfer coefficients in APG flow in comparison to ZPG flow in the same longitudinal coordinate.

**Heat transfer coefficient.** According to the results of an experimental study (Fig. 11), the heat transfer coefficients  $\alpha$ ,  $\text{W/m}^2\text{K}$  are considerably influenced by the pressure gradient. The heat transfer coefficient in the channel with the minimum divergence angle was up to

1.25 times higher in comparison with the value in the channel with the maximum divergence angle in the same section. This increase is due to a Mach number decrease and an increase in the mass flux  $(\rho \cdot U)_{av}$  as the divergence angle decreases and the APG increases.

The Stanton number  $St$  (Fig. 12) behaves differently since it is influenced only by the Mach number,  $\beta_K$ , and  $Re^*$ . In the investigated flow region, before the shock, the numerical and experimental data for heat transfer show tendencies similar to those observed earlier for the skin friction coefficient.

**Temperature recovery factor.** According to the published data [6], the temperature recovery factor in a developed ZPG TBL is near-constant in a wide range of parameters and amounts to  $r \approx 0.89 \pm 0.01$  for the air. Distributions of the experimental and numerical recovery factor  $r$  along the length of the investigated region for different divergence angles are shown in Fig. 13. It can be noted that in the investigated region the calculated and experimental values of  $r$  coincide and are independent of the pressure gradient. The temperature recovery factor value corresponds to the ZPG TBL conditions.

**Extended Reynolds analogy.** As noted in the Introduction, the value of the Reynolds analogy factor  $s$  for ZPG boundary layers of gases with a Prandtl number  $Pr \approx 1$  is determined by their physical properties and is equal to 1.16 for air. A streamwise pressure gradient, compressibility effect, and high-rate dissipation result in a difference in the equations of motion and energy and a difference in the development of the thermal and dynamic boundary layers. In these flows the Reynolds analogy can be violated, as regards both the heat transfer ( $s > 1$ ) and skin friction ( $s < 1$ ).

The supersonic nozzles of all channels were identical (Fig. 2). This fact determines the similarity of histories for the channels with different divergence angles (Fig. 8). The preliminary flow acceleration in the supersonic nozzle with  $\beta_K < -0.5$  leads to an increase in the skin friction coefficient  $c_f$  and a decrease in the heat transfer coefficient  $St$ . Thus, even before the beginning of APG the Reynolds analogy is violated toward an increase of skin friction. The value of the Reynolds analogy factor  $s$  at the nozzle exit amounted to 0.83, which is considerably lower than its value for the ZPG ( $s \approx 1.16$ ) (Fig. 14a). It can be noted that the predominant influence of the flow history and the inaccessibility of the equilibrium state corresponding to the current values of  $Re^*$  and  $\beta_K$  is analogous to the situation described in Refs. [16–20]. As the boundary layer develops, the quantity  $s$  increases and tends to its ZPG level, which is the consequence of the boundary layer recovery.

According to the results of the DNS calculations [18], supersonic boundary layers attain an equilibrium state (and the corresponding values of the skin friction and heat transfer coefficients) considerably slower than the subsonic one. In this case, the equilibrium along the entire APG region cannot be achieved in all flow regimes. The rate of the recovery of the Reynolds analogy factor to its equilibrium value reduces with a decrease in the channel divergence angle and an increase in the

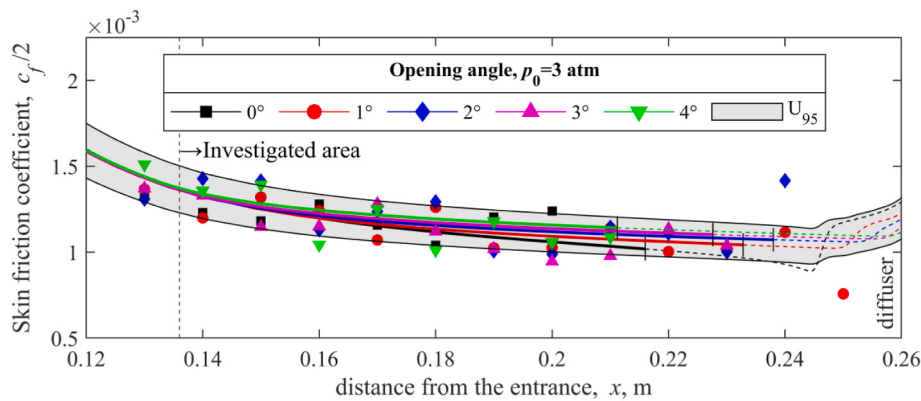
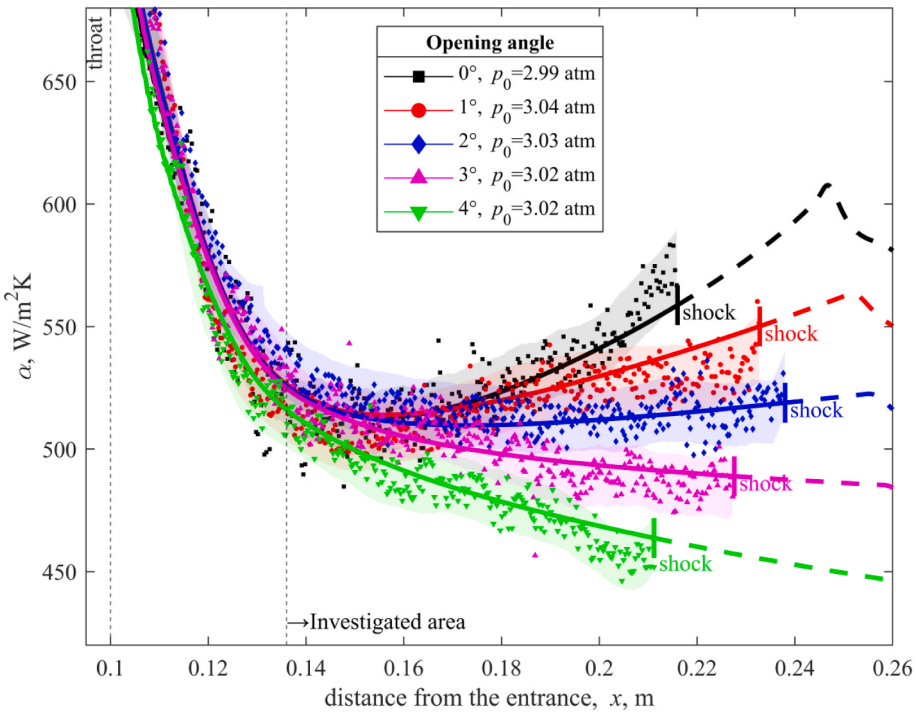
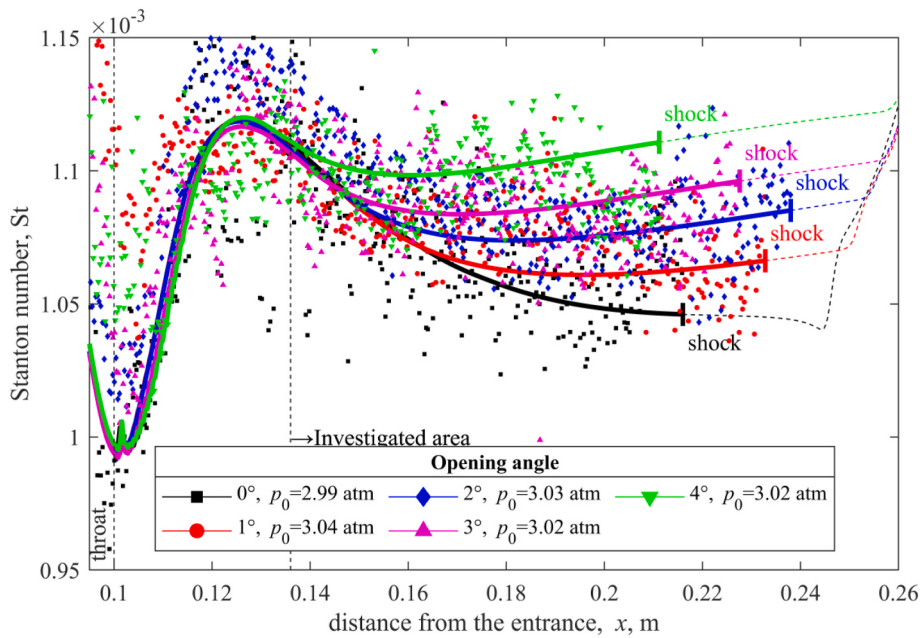


Fig. 10. Variation of the skin friction coefficient in the channels under study at  $p_0 \approx 3$  atm. Points present experimental data, lines present calculations.



**Fig. 11.** Heat transfer coefficient  $\alpha$ ,  $\text{W}/\text{m}^2\cdot\text{K}$  in the investigated channels at stagnation pressure:  $p_0 \approx 3.0 \text{ atm}$ . The shaded region and points present experimental data, lines present calculations.



**Fig. 12.** Stanton number St in the investigated channels. Points present experimental data, lines present calculations.

APG. In an equilibrium boundary layer an increase in  $s$  amounts to 40% in relation to the ZPG flow with the same longitudinal coordinate  $x$ . However, the actual increase of  $s$  in the investigated channel (to the  $s$  value in the channel with the divergence angle of  $3^\circ$ ) is considerably lower and amounts to only 10 % according to the experimental and numerical results. This is particularly noticeable in the relative value of  $s$  presented in Fig. 14b. The value of  $s$  is normalized to the equilibrium value for a corresponding  $\beta_K$  and Reynolds number  $Re^*$ .

According to numerical result, the effect of the stagnation pressure (unit Reynolds number) on the Reynolds analogy factor is almost absent,

as  $p_0$  varies the limits of  $p_0 = 2.20 \dots 3.02 \text{ atm}$  (not shown in Fig. 14). The realized change in the Reynolds number  $Re^*$  in the inlet section of the investigated region leads to a change in  $s$  and  $s/s_{eq}$  of less than a percent, which is significantly less than the accuracy of both experimental and numerical values.

The boundary layer development can be illustrated by plotting the dependence of the Reynolds analogy factor on the pressure gradient parameter  $\beta_K$  (Fig. 15) for the investigated and equilibrium flows. The calculated and experimental values are presented for all geometries and  $p_0 = 3.02 \text{ atm}$ , up to the shock section. As noted above, the boundary

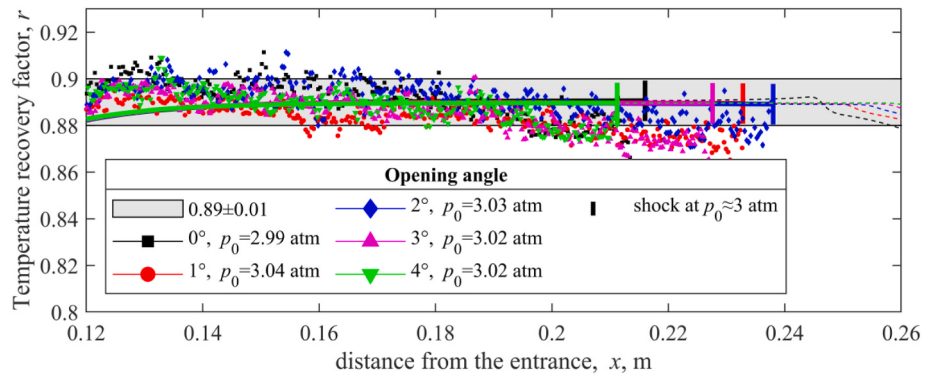


Fig. 13. Temperature recovery factor  $r$  in the investigated channels. Points present experimental data, lines present calculations.

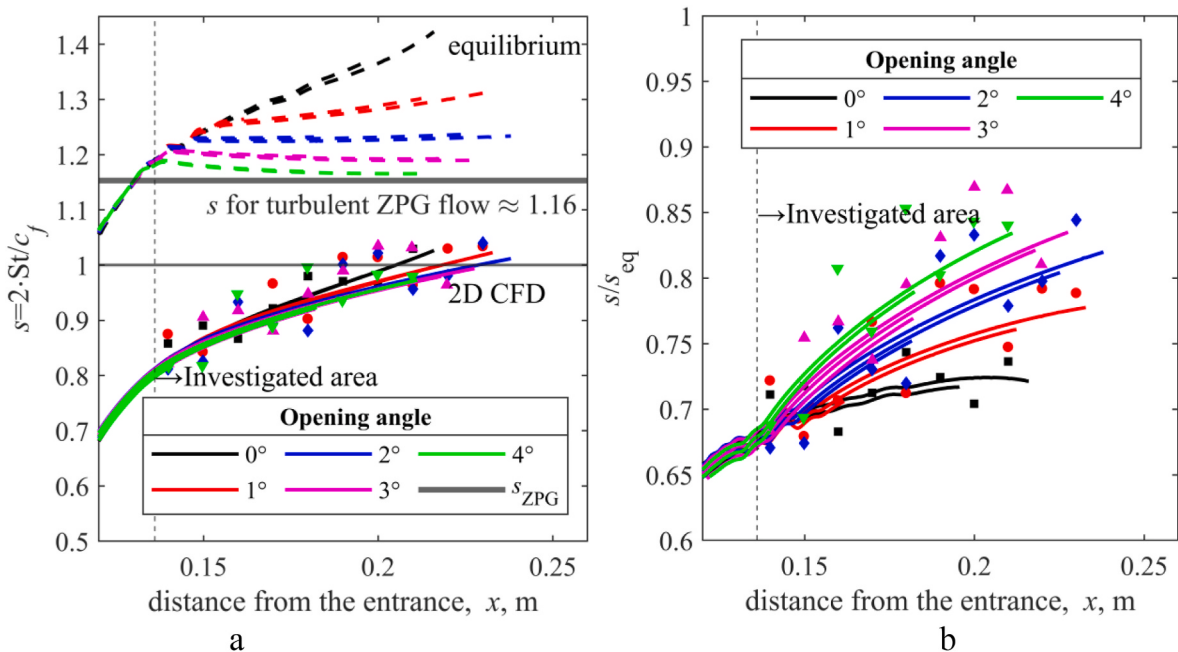


Fig. 14. Reynolds analogy factor  $s$  along the length of the APG region in the investigated channels: (a), absolute value  $s$  and (b), reduced to the corresponding equilibrium value,  $s/s_{\text{eq}}$ . Points present experimental data Continuous lines present 2D calculations and broken lines present the solution [12]. The values are presented before the shock.

layer is far from equilibrium, and in the parameter range under study, the Reynolds analogy factor is only slightly greater than unity. As the boundary layer develops, the quantity  $s(\beta_K)$  increases. For the moderate pressure gradient, the value of  $s$  repeats the equilibrium tendency of increasing with an increase in  $\beta_K$ . This trend is imposed by the violation of the Reynolds analogy in the direction of skin friction, which is due to the flow history effect (the non-equilibrium acceleration). Even though that the highest  $s$  values are achieved in the channel with the highest APG, the flow regimes are far from equilibrium and they were not realized in experiments due to the shock. Their deviations from equilibrium values increase with the longitudinal coordinate  $x$ .

For a channel with the highest APG corresponding to zero divergence angle, the value of the normalized Reynolds analogy factor  $s/s_{\text{eq}}$  begins to decrease (while it continues to increase in the absolute value) starting at the coordinate  $x = 0.19 \text{ m}$  (Fig. 15b). This indicates that the flow has no time to react to the imposed pressure gradient. This also can be seen in the  $s(\beta_K)$  plot (Fig. 15a). Thus, the quantity  $s$  increases but starts to lag behind the corresponding equilibrium value (Fig. 15b) as the APG increases, together with the length of its imposition.

An increase in  $s$  is highest at the beginning of the APG section and then reduces for all divergence angles. With the decrease in  $\beta_K$ , it

becomes possible to approach the equilibrium values most closely. Nonetheless, equilibrium was attained for neither flow regime. The maximum values of  $s$  were independent of  $\beta_K$  and turned out to be about 15% lower for the channels with near-ZPG conditions and about 28% lower for the channel with the highest APG compared to equilibrium values. Consequently, the value of  $s/s_{\text{eq}}$  decreased as the divergence angle decreased (Fig. 15b).

Summing up the above-said we may state that flow in a supersonic slot channel with APG downstream of the FPG region (supersonic nozzle) is accompanied by:

- a decrease in the mass flux  $(\rho \cdot U)_{\text{av}}$  at the expense of an increase in the supersonic channel cross-section affects the heat transfer coefficient  $\alpha$  while the Stanton number  $St$  and skin friction coefficient  $c_f$  remain near the constant;
- an increase in  $\Psi_M$ ,  $c_f$  and  $St$  values, while the Reynolds analogy factor  $s$  remains constant caused by a decrease in the Mach number  $M_\pi$  and the compressibility effect;
- only the direct and history effect of pressure gradient has an impact on the values of the Reynolds analogy factor  $s$ . The  $s$  increases, as the boundary layer grows. However, in the flows considered  $s$  is much

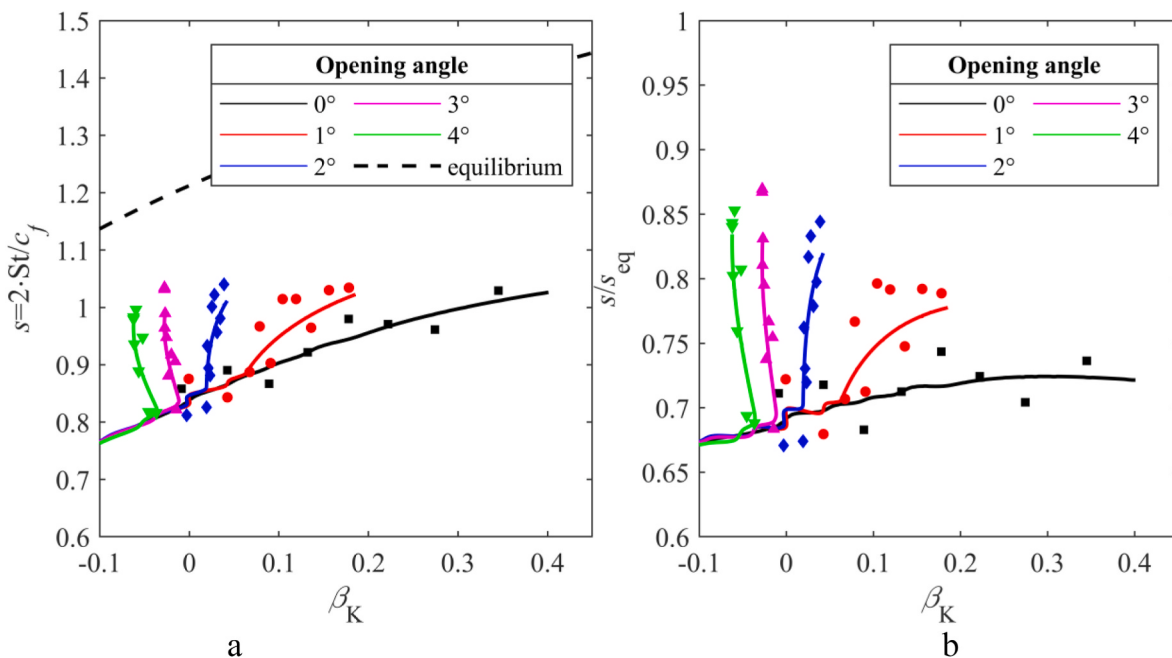


**Fig. 15.** Reynolds analogy factor  $s$  in the channels under investigation as a function of the pressure gradient parameter: (a), absolute value  $s$  and (b), reduced to the corresponding equilibrium value,  $s/s_{eq}$ . Points present experimental data Continuous lines present relate to 2D calculations and broken lines present correspond to the solution [12]. The values are presented before the shock.

lower than the equilibrium values. The maximum attained value is independent of  $\beta_K$  and amounted to  $s \approx 1.0$  in the  $\beta_K$  range realized in the experiments;

- the increase in the APG value leads to shifting the shock wave toward the critical cross-section and a reduction in the length of the investigated region of channels.

While the APG effect on the integral parameters of the boundary layer within the investigated range of parameters is not greater than the influence of the factors mentioned above. Its combination leads to an increase in the values of the Reynolds analogy factor  $s$ .

## 5. Conclusion

The APG effect on the parameters of the thermal and dynamic boundary layers in a supersonic slot channel was experimentally investigated. Five channels with different geometries of supersonic regions and the same supersonic nozzle were considered. Variations in the pressure gradient were reached by the imposition of an area change on the supersonic flow with skin friction. The shock-free flow deceleration in a channel was realized. The skin friction coefficient was determined using the Shapiro-Hawthorne method, while the heat transfer coefficient and temperature recovery factor were measured using the transient heat transfer method. The parameter  $\beta_K$  [28] was taken for the pressure gradient parameter. For the flow parameters realized in the experiment, we considered the solution of equations of the two-dimensional turbulent compressible boundary layer using the SST turbulence model.

The following conclusions are made:

- The pressure gradient parameter  $\beta_K$  does not allow the unique determination of the boundary layer properties owing to the presence of the flow history due to the FPG in the supersonic nozzle;
- The APG does not affect the temperature recovery factor  $r$  in the realized flows;
- The applicability of the solutions of the boundary layer equations in the class of the problems under consideration was shown. The

experimental and numerical results were in agreement up to the shock formation zone;

- The presence of a nozzle section (FPG region) shifts the values of the Reynolds analogy factor toward an increase in skin friction;
- For channels with nozzles, in the supersonic region, the history effects predominate over the direct impact of the APG on the Reynolds analogy factor. These boundary layers are far from equilibrium;
- The estimation of flow acceleration influence in the nozzles is limited due to the inability to formalize the direct effect using the parameter  $\beta$  or  $\beta_K$ , due to the formation of equilibrium boundary layers is impossible for a typical acceleration level. It requires further investigation.

## CRediT authorship contribution statement

**N.A. Kiselev:** Writing – original draft, Methodology, Investigation, Conceptualization. **N.S. Malastowski:** Writing – review & editing, Writing – original draft, Visualization, Software, Data curation, Conceptualization. **A.G. Zditovets:** Supervision, Resources, Project administration, Methodology, Conceptualization. **Yu.A. Vinogradov:** Supervision, Methodology, Formal analysis, Data curation.

## Declaration of competing interest

The authors declare the following financial interests/personal relationships which may be considered as potential competing interests: Nickolay Kiselev reports financial support was provided by Russian Science Foundation. If there are other authors, they declare that they have no known competing financial interests or personal relationships that could have appeared to influence the work reported in this paper.

## Data availability

Data will be made available on request.

## Acknowledgments

The study was supported by the Russian Science Foundation (project no. 19-79-10213), <https://rscf.ru/en/project/19-79-10213/>.

## References

- [1] H. Schlichting, *Boundary Layer Theory*, McGraw-Hill, New York, 1979.
- [2] F.H. Clauser, Turbulent boundary layers in adverse pressure gradients, *J. Aeronaut. Sci.* 21 (1954) 91–108, <https://doi.org/10.2514/8.2938>.
- [3] N.A. Kiselev, A.I. Leontiev, Y.A. Vinogradov, et al., Heat transfer and skin-friction in a turbulent boundary layer under a non-equilibrium longitudinal adverse pressure gradient, *Int. J. Heat Fluid Flow* 89 (2021) 108801, <https://doi.org/10.1016/j.ijheatfluidflow.2021.108801>.
- [4] W.J. Devenport, K.T. Lowe, Equilibrium and non-equilibrium turbulent boundary layers, *Prog. Aero. Sci.* 131 (2022) 100807, <https://doi.org/10.1016/j.paerosci.2022.100807>.
- [5] S.S. Kutateladze, A.I. Leontiev, *Heat Transfer, Mass Transfer, and Friction in Turbulent Boundary Layer*, Taylor and Francis, New York, 1990.
- [6] M.W. Rubesin, A modified Reynolds analogy for the compressible turbulent boundary layer on a flat plate, *NACA Technical Note 2917* (1953) 1–21.
- [7] R.L. Webb, Performance evaluation criteria for use of enhanced heat transfer surfaces in heat exchanger design, *Int. J. Heat Mass Tran.* 24 (1981) 715–726, [https://doi.org/10.1016/0017-9310\(81\)90015-6](https://doi.org/10.1016/0017-9310(81)90015-6).
- [8] F.H. Clauser, The turbulent boundary layer, *Adv. Appl. Mech.* 4 (1956) 1–51, [https://doi.org/10.1016/S0065-2156\(08\)70370-3](https://doi.org/10.1016/S0065-2156(08)70370-3).
- [9] G.L. Mellor, D.M. Gibson, Equilibrium turbulent boundary layers, *J. Fluid Mech.* 24 (1966) 225–253, <https://doi.org/10.1017/S0022112066000612>.
- [10] M. Skote, D.S. Henningson, Direct numerical simulation of adverse pressure gradient turbulent boundary layers, *Fluid Mech. Its Appl.* 46 (1998) 171–174, [https://doi.org/10.1007/978-94-011-5118-4\\_42](https://doi.org/10.1007/978-94-011-5118-4_42).
- [11] P.E. Skåre, P.A. Krogstad, A turbulent equilibrium boundary layer near separation, *J. Fluid Mech.* 272 (1994) 319–348, <https://doi.org/10.1017/S0022112094004489>.
- [12] R.M.C. So, Pressure gradient effects on Reynolds analogy for constant property equilibrium turbulent boundary layers, *Int. J. Heat Mass Tran.* 37 (1994) 27–41, [https://doi.org/10.1016/0017-9310\(94\)90159-7](https://doi.org/10.1016/0017-9310(94)90159-7).
- [13] C. Sanmiguel Vila, R. Vinuesa, S. Discetti, et al., Experimental realisation of near-equilibrium adverse-pressure-gradient turbulent boundary layers, *Exp. Therm. Fluid Sci.* 112 (2020) 109975, <https://doi.org/10.1016/j.exthermflusci.2019.109975>.
- [14] N. Tetrov, Approximate calculation of Reynolds analogy for turbulent boundary layer with pressure gradient 7 (1969) 1079–1085.
- [15] B.S. Stratford, An experimental flow with zero skin friction throughout its region of pressure rise, *J. Fluid Mech.* 5 (1959) 17–35, <https://doi.org/10.1017/S0022112059000027>.
- [16] P. Bradshaw, D.H. Ferriss, *Nat. Phys. Lab. Aero Rept. (1145)* (1965).
- [17] A. Bobke, R. Vinuesa, R. Örlü, P. Schlatter, History effects and near equilibrium in adverse-pressure-gradient turbulent boundary layers, *J. Fluid Mech.* 820 (2017) 667–692, <https://doi.org/10.1017/jfm.2017.236>.
- [18] C. Wenzel, T. Gibis, M. Kloker, U. Rist, Reynolds analogy factor in self-similar compressible turbulent boundary layeres with pressure gradients, *J. Fluid Mech.* 907 (2020), <https://doi.org/10.1017/jfm.2020.876>.
- [19] P.R. Spalart, J.H. Watmuff, Experimental and numerical study of a turbulent boundary layer with pressure gradients, *J. Fluid Mech.* 249 (1993) 337, <https://doi.org/10.1017/S002211209300120X>.
- [20] Y. Nagano, M. Tagawa, T. Tsuji, Effects of adverse pressure gradients on mean flows and turbulence statistics in a boundary layer, in: F. Durst, R. Friedrich, B. E. Launder, et al. (Eds.), *Turbulent Shear Flows*, vol. 8, Springer, Berlin, Heidelberg, 1993, pp. 7–21.
- [21] Y. Maciel, K.S. Rossignol, J. Lemay, A study of a turbulent boundary layer in stalled-airfoil-type flow conditions, *Exp. Fluid* 41 (2006) 573–590, <https://doi.org/10.1007/s00348-006-0182-1>.
- [22] L.H. Back, R.F. Cuffel, P.F. Massier, Laminarization of a turbulent boundary layer in nozzle flow—boundary layer and heat transfer measurements with wall cooling, *J. Heat Tran.* 92 (1970) 333–344, <https://doi.org/10.1115/1.3449668>.
- [23] K. Mastanaiah, Prediction of skin-friction and heat transfer from compressible turbulent boundary layers in rocket nozzles, *Int. J. Heat Mass Tran.* 21 (1978) 1403–1410, [https://doi.org/10.1016/0017-9310\(78\)90204-1](https://doi.org/10.1016/0017-9310(78)90204-1).
- [24] K.R. Mutama, H. Iacovides, The Investigation of developing flow and heat transfer in a long converging duct, *J. Heat Tran.* 115 (1993) 897–903, <https://doi.org/10.1115/1.2911385>.
- [25] J. Bons, A critical assessment of Reynolds analogy for turbine flows, *J. Heat Tran.* 127 (2005) 472–485, <https://doi.org/10.1115/1.1861919>.
- [26] R.E. Mayle, The 1991 IGTI scholar lecture: the role of laminar-turbulent transition in gas turbine engines, *J. Turbomach.* 113 (1991) 509–536, <https://doi.org/10.1115/1.2929110>.
- [27] M. Dong, H. Huang, Y. Feng, J. Qin, Investigation of the flow and heat transfer performance of supercritical pressure hydrocarbon fuel in a novel rotating internal trapezoidal expansion channel, *Int. Commun. Heat Mass Tran.* 147 (2023) 106941, <https://doi.org/10.1016/j.icheatmasstransfer.2023.106941>.
- [28] J.E. Lewis, R.L. Gran, T. Kubota, An experiment on the adiabatic compressible turbulent boundary layer in adverse and favourable pressure gradients, *J. Fluid Mech.* 51 (1972) 657–672, <https://doi.org/10.1017/S0022112072001296>.
- [29] Q.C. Wang, Z.G. Wang, Y.X. Zhao, On the impact of adverse pressure gradient on the supersonic turbulent boundary layer, *Phys. Fluids* 28 (2016), <https://doi.org/10.1063/1.4968527>.
- [30] W.B. Sturek, J.E. Danberg, Supersonic turbulent boundary layer in adverse pressure gradient. Part II: data analysis, *AIAA J.* 10 (1972) 630–635, <https://doi.org/10.2514/3.50167>.
- [31] D.H. Lee, Compressible turbulent boundary layer in strong adverse pressure gradient, *AIAA J.* 21 (1983) 632–633.
- [32] A.J. Ladberman, Adverse pressure gradient effects on supersonic boundary-layer turbulence, *AIAA J.* 18 (1980) 1186–1195, <https://doi.org/10.2514/3.50870>.
- [33] C. Wenzel, T. Gibis, M. Kloker, U. Rist, Self-similar compressible turbulent boundary layers with pressure gradients. Part 1. Direct numerical simulation and assessment of Morkovin's hypothesis, *J. Fluid Mech.* 880 (2019) 239–283, <https://doi.org/10.1017/jfm.2019.670>.
- [34] A.I. Leontiev, A.G. Zditovets, N.A. Kiselev, et al., Experimental investigation of energy (temperature) separation of a high-velocity air flow in a cylindrical channel with a permeable wall, *Exp. Therm. Fluid Sci.* 105 (2019) 206–215, <https://doi.org/10.1016/j.exthermflusci.2019.04.002>.
- [35] T. Houra, Y. Nagano, Effects of adverse pressure gradient on heat transfer mechanism in thermal boundary layer, *Int. J. Heat Fluid Flow* 27 (2006) 967–976, <https://doi.org/10.1016/j.ijheatfluidflow.2006.03.019>.
- [36] Y. Nagano, T. Tsuji, T. Houra, Structure of turbulent boundary layer subjected to adverse pressure gradient, *Int. J. Heat Fluid Flow* 19 (1998) 563–572, [https://doi.org/10.1016/S0142-727X\(98\)10013-9](https://doi.org/10.1016/S0142-727X(98)10013-9).
- [37] A. E. Samuel, P.N. Joubert, A boundary layer developing in an increasingly adverse pressure gradient, *J. Fluid Mech.* 66 (1974) 481, <https://doi.org/10.1017/S0022112074000322>.
- [38] H. Rae W, A. Pope, *Low-speed Wind Tunnel Testing*, second ed., Jonh Wiley & Sons, New York, 1984.
- [39] N.A. Kiselev, N.S. Malastowski, Y.A. Vinogradov, A.G. Zditovets, Experimental and numerical study of heat transfer under laminarization condition in a small size supersonic nozzle, *Int. J. Therm. Sci.* 187 (2023) 108182, <https://doi.org/10.1016/j.ijthermalsci.2023.108182>.
- [40] A.M. Ovsannikov, U.G. Pirumov, E.M. Pletneva, G.S. Roslyakov, *Atlas Ploskih Sopel*, Moscow University Press, Moscow, 1976.
- [41] A.H. Shapiro, *The Dynamics and Thermodynamics of Compressible Fluid Flow*, The Ronald Press Company, New York, 1953.
- [42] A.G. Zditovets, N. Kiselev, Y.A. Vinogradov, S. Popovich, Adiabatic wall temperature in the supersonic flow of moist air with spontaneous condensation, *Exp. Therm. Fluid Sci.* 150 (2024) 111057, <https://doi.org/10.1016/j.exthermflusci.2023.111057>.
- [43] A.H. Shapiro, W.R. Hawthorne, The mechanics and thermodynamics of steady one-dimensional gas flow, *J. Appl. Mech. Trans. ASME* 14 (1947) A317–A336, <https://doi.org/10.1115/1.4009740>.
- [44] J.E. Bialokoz, O.A. Saunders, Heat transfer in pipe flow at high speeds, *Proc. Inst. Mech. Eng.* 170 (1956) 389–406, [https://doi.org/10.1243/pime\\_proc\\_1956\\_170\\_038\\_02](https://doi.org/10.1243/pime_proc_1956_170_038_02).
- [45] R.J. Moffat, Describing the uncertainties in experimental results, *Exp. Therm. Fluid Sci.* 1 (1988) 3–17, [https://doi.org/10.1016/0894-1777\(88\)90043-X](https://doi.org/10.1016/0894-1777(88)90043-X).
- [46] J.C. Williams, Viscous compressible and incompressible flow in slender channels, *AIAA J.* 1 (1963) 186–195, <https://doi.org/10.2514/3.1488>.
- [47] F.R. Menter, Two-equation eddy-viscosity turbulence models for engineering applications, *AIAA J.* 32 (1994) 1598–1605, <https://doi.org/10.2514/3.12149>.
- [48] B. Weigand, J.R. Ferguson, M.E. Crawford, An extended Kays and Crawford turbulent Prandtl number model, *Int. J. Heat Mass Tran.* 40 (1997) 4191–4196, [https://doi.org/10.1016/S0017-9310\(97\)00084-7](https://doi.org/10.1016/S0017-9310(97)00084-7).
- [49] D. Anderson, J.C. Tannehill, R.H. Pletcher, *Computational Fluid Mechanics and Heat Transfer*, third ed., CRC Press, 2016.